Author's response to co-editor:

Thank you very much for your comment! You helped us improve this study significantly.

Comment: The referee asked why the (negative) deposition flux should INcrease when the SOC increases (table 5 and 7). This question is based on the assumption that higher SOC provides more substrate for CO formation in the soil, which would DEcrease the soil-atmosphere gradient and DEcrease the deposition flux. There must be one process in your model that leads to an increase in the deposition flux.

You argue now with time step arguments, which apparently play a role, but even with a short timestep the sign of the flux change remains the same, even if the magnitude is reduced. I think it is still required that you explain the physical basis of the effect. And then it would also be good if you can argue a bit more quantitatively why the timestep has such a large influence (and that this then does not affect other results of your model).

Response: Thank you for your suggestions to improve the sensitivity analysis presented in the paper. In this revision, we removed Table 7 to avoid distraction from our main focus. We have also revised the sensitivity test (Table 5) by using SOC ±5% instead of ±30% (not a realistic variation), since during our century-scale simulations, the SOC will not change beyond 4% within a century. This small variation of SOC did not affect CO consumption drastically, in contrast to the large effects due to sudden high and unrealistic SOC changes in the original sensitivity test. Consequently, our other results of the global CO consumption simulations were not significantly affected by small variations of SOC (less than 4%).

We followed your suggestion to mainly explain the physical basis of the effect in this revision. Please find our changes for Table 5 and revisions on lines 126, 296, 364, 367, and 404-405 for sensitivity test results and explanation in Section 4.3, lines from 452 to 469. We quoted the revised text here

"Fourth, from sensitivity test (Table 5) we notice that SOC increasing (5%) resulted in a

net flux increase (2.57%). The SOC increase enhanced CO production (Equation 3), CO concentrations (Equation 1), and CO oxidation (Equation 2). When the change of total oxidation is larger than the difference between the change of total production and the change of total soil CO concentration (Equation 1), the estimate of the net flux change is negative (from atmosphere to soil) using a mass balance approach (Section 2.2), leading to a 2.57% increase in net flux in our SOC sensitive test. This is due to the fact that CO production (Equation 3) is calculated independently from oxidation calculation (Equation 2). This will not influence our other results since SOC varies slightly during our simulation periods with only a 3% increase from 1900 to 2013 (Figure 4d) and up to a 4% increase from 2014 to 2100 (Figure 6g). This artifact problem in SOC sensitivity test can be alleviated using a very fine time step (e.g., 1 second), because CO concentrations will change slightly within the short time, allowing net flux roughly equals the difference between production and oxidation within the short time step. If the change of production is bigger than the change of oxidation, the change of net flux will be positive, leading to a decrease of deposit to soil. The downside is that running the model at one second time step will require significantly high computing time."

Global Soil Consumption of Atmospheric Carbon Monoxide: An Analysis Using a Process-Based Biogeochemistry Model

Licheng Liu[1], Qianlai Zhuang[1,2], Qing Zhu[1,3], Shaoqing Liu[1,4], Hella van Asperen[5], Mari Pihlatie[6,7]

[1]Department of Earth, Atmospheric, Planetary Sciences, Purdue University, West Lafayette, IN 47907, USA

[2]Department of Agronomy, Purdue University, West Lafayette, IN 47907, USA

[3] Climate Sciences Department, Climate & Ecosystem Sciences Division, Lawrence Berkeley National Laboratory, Berkeley, CA 94720, USA

[4]Department of Earth Sciences, University of Minnesota, Minneapolis, MN, 55455,USA

[5]Institute of Environmental Physics, University of Bremen, Otto-Hahn-Allee 1, Bremen, 28359, Germany

[6]Department of Physics, University of Helsinki, P.O. Box 48, 00014 University of Helsinki, Finland

[7]Department of Forest Sciences, P.O. Box27, 00014 University of Helsinki, Finland

Correspondence to: Qianlai Zhuang(qzhuang@purdue.edu)

Abstract: Carbon monoxide (CO) plays an important role in controlling the oxidizing capacity of the atmosphere by reacting with OH radicals that affect atmospheric methane (CH_4) dynamics. We develop a process-based biogeochemistry model to quantify CO exchange between soils and the atmosphere with a 5-minute internal time step at the global scale. The model is parameterized using CO flux data from the field and laboratory experiments for eleven representative ecosystem types. The model is then extrapolated to the global terrestrial ecosystems using monthly climate forcing data. Global soil gross consumption, gross production, and net flux of the atmospheric CO are estimated to be from -197 to -180, 34 to 36, and -163 to -145 Tg CO yr^{-1} (1Tg = 10^{12} g), respectively, driven with satellite-based atmospheric CO concentration data during 2000-2013. Tropical evergreen forest, savanna and deciduous forest areas are the largest sinks at 123 Tg CO yr^{-1}. Soil CO gross consumption is sensitive to air temperature and atmospheric CO concentration while gross production is sensitive to soil organic carbon (SOC) stock and air temperature. By assuming that the spatially-distributed atmospheric CO concentrations (~128 ppbv) are not changing over time, global mean CO net deposition velocity is estimated to be 0.16-0.19 mm s^{-1} during the 20th century. Under the future climate scenarios, the CO deposition velocity will increase at 0.0002-0.0013 mm s^{-1} yr^{-1} during 2014-2100, reaching 0.20-0.30 mm s^{-1} by the end of the 21st century, primarily due to increasing temperature. Areas near the equator, Eastern US, Europe and eastern Asia will be the largest sinks due to optimum soil moisture and high temperature. The annual global soil net flux of atmospheric CO is primarily controlled by air temperature, soil temperature, SOC and atmospheric CO concentrations, while its monthly variation is mainly determined by air temperature, precipitation, soil temperature and soil moisture.

1. Introduction

Carbon monoxide (CO) plays an important role in controlling the oxidizing capacity of the atmosphere by reacting with OH radicals (Logan et al., 1981; Crutzen, 1987; Khalil & Rasmussen, 1990; Prather et al., 1995; Prather & Ehhalt, 2001). CO in the atmosphere can directly and indirectly influence the fate of critical greenhouse gases such as methane (CH_4) and ozone (O_3) (Tan and Zhuang, 2012). Although CO itself absorbs only a limited amount of infrared radiation from the Earth, the cumulative

indirect radiative forcing of CO may be even larger than that of the third powerful greenhouse gas, nitrous oxide (N_2O, Myhre et al., 2013). Current estimates of global CO emissions from both anthropogenic and natural sources range from 1550 to 2900 Tg CO yr^{-1}, which are mainly from anthropogenic and natural direct emissions and from the oxidation of methane and other Volatile Organic Compounds (VOC) (Prather et al., 1995; Khalil et al., 1999; Bergamaschi et al., 2000; Prather & Ehhalt, 2001, Stein et al., 2014). Chemical consumption of CO by atmospheric OH and the biological consumption of CO by soil microbes are two major sinks of the atmospheric CO (Conrad, 1988; Lu & Khalil, 1993; Yonemura et al., 2000; Whalen & Reeburgh, 2001).

Soils are globally considered as a major sink for CO due to microbial activities (Whalen and Reeburgh, 2001; King and Weber, 2007). A diverse group of soil microbes including carboxydotrophs, methanotrophs and nitrifiers are capable of oxidizing CO (King and Weber, 2007). Annually, 10-25% of total earth surface CO emissions were consumed by soils (Sanhueza et al., 1998; King, 1999a; Chan & Steudler, 2006). Potter et al. (1996) reported the global soil consumption to be from -50 to -16 Tg CO yr^{-1} (negative values represent the uptake from the atmosphere to soil), by using a single-box model over the upper 5 cm of soils. All existing estimates have large uncertainties and range from -640 to -16 Tg CO yr^{-1} (Sanhueza et al., 1998; King, 1999; Bergamaschi et al., 2000). Similarly, the estimates of CO dry deposition velocities also have large uncertainties and range from 0 to 4.0mm s^{-1} (here positive values are amount of deposition to soils, King, 1999a; Castellanos et al., 2011). Soils also produce CO mainly via abiotic processes such as thermal- and photo-degradation of organic matter or plant materials (Conrad and Seiler, 1985b; Tarr et al., 1995; Schade et al., 1999; Derendorp et al., 2011; Lee et al., 2012; van Asperen et al., 2015; Fraser et al., 2015, Pihlatie et al., 2016), except for a few cases of anaerobic formation. Photo-degradation is identified as radiation-dependent degradation due to absorbing radiation (King et al., 2012). Thermal-degradation is identified as the temperature-dependent degradation of carbon in the absence of radiation and possibly oxygen (Derendorp et al., 2011; Lee et al., 2012; van Asperen et al., 2015; Pihlatie et al., 2016). These major soil CO production processes, together with soil CO consumption processes, have not been adequately modeled in global soil CO budget estimates.

To date, most top-down atmospheric models applied a dry deposition scheme based on the resistance model of Wesely (1989). Such schemes provided a wide range of dry deposition velocities (Stevenson et al., 2006). Only a few models (MOZART-4, Emmons et al., 2010; CAM-chem, Lamarque et al., 2012) have extended their dry deposition schemes with a parameterization for CO and H_2 uptake through oxidation by soil microbes following the work of Sanderson et al. (2003), which itself was based on extensive measurements from Yonemura et al. (2000). Potter et al. (1996) developed a bottom-up model to simulate CO consumption and production at the global scale. This model is a single box model, only considers top 5cm depth of soil and does not have explicit microbial factors, which might have underestimated CO consumption (Potter et al., 1996; King, 1999a). Current bottom-up CO modeling approaches are mostly based on a limited number of CO *in situ* observations or laboratory studies to quantify regional and global soil consumption (Potter et al., 1996; Sanhueza et al., 1998; Khalil et al., 1999; King, 1999a; Bergamaschi et al., 2000; Prather & Ehhalt, 2001). To our knowledge, no detailed process-based model of soil-atmospheric exchange of CO has been published in the recent 15 years. One reason is that there is an incomplete understanding of biological processes of uptake (King & Weber, 2007; Vreman et al., 2011; He and He, 2014; Pihlatie et al., 2016). Another reason is that there is lack of long-term CO flux measurements for different ecosystem types to calibrate and evaluate the models. CO flux measurements are mostly from short-term field observations or laboratory experiments (e.g. Conrad and Seiler, 1985a; Funk et al., 1994; Tarr et al., 1995; Zepp et al., 1997; Kuhlbusch et al., 1998; Moxley and Smith, 1998; Schade et al., 1999; King and Crosby, 2002; Varella et al., 2004; Lee et al., 2012; Bruhn et al., 2013; van Asperen et al., 2015). The first study to report long-term and continuous field measurements of CO flux over grasslands using a micrometeorological eddy covariance (EC) method is Pihlatie et al. (2016).

To improve the quantification of the global soil CO budget for the period 2000-2013 and CO deposition velocity for the 20th and 21st centuries, this study developed a CO dynamics module (CODM) embedded in a process-based biogeochemistry model, the Terrestrial Ecosystem Model (TEM) (Zhuang et al., 2003, 2004, 2007). CODM was then calibrated and evaluated using laboratory experiments and field measurements for

different ecosystem types. The atmospheric CO concentration data from MOPITT (Gille, 2013) were used to drive model simulations from 2000 to 2013. A set of century-long simulations of 1901-2100 were also conducted using the atmospheric CO concentrations estimated with an empirical function (Badr & Probert, 1994; Potter et al., 1996). Finally, the effects of multiple forcings on the global CO consumption and production, including the changes of climate and atmospheric CO concentrations at the global scale were evaluated with the model.

2. Method

2.1 Overview

We first developed a daily soil CO dynamics module (CODM) that considers: (1) soil-atmosphere CO exchange and diffusion process between soil layers, (2) consumption by soil microbial oxidation, (3) production by soil chemical oxidation, and (4) the effects of temperature, soil moisture, soil CO substrate and surface atmospheric CO concentration on these processes. Second, we used the observed soil temperature and moisture to evaluate TEM hydrology module and soil thermal module in order to estimate soil physical variables. Then we used the data from laboratory experiments and CO flux measurements to parameterize the model using the Shuffled Complex Evolution (SCE-UA) method (Duan et al., 1993). Finally, the model was extrapolated to the globe at a 0.5° by 0.5° resolution. We conducted three sets of model experiments to investigate the impact of climate and atmospheric CO concentrations on soil CO dynamics: 1) simulations for 2000-2013 with MOPITT satellite atmospheric CO concentration data; 2)simulations for 1901-2100 with constant atmospheric CO concentrations estimated from an empirical function and the historical climate data (1901-2013) and three future climate scenarios (2014-2100); and 3) Eight sensitivity simulations by changing a) constant CO surface concentrations ± 30%, b) SOC ±5~~30~~%, c) precipitation ±20% and d) air temperature ± 3°C for each pixel, respectively, while holding other forcing data as they were, during 1999-2000.

2.2 Carbon Monoxide Dynamics Module (CODM)

Embedded in TEM (Figure 1), CODM is mainly driven by: (1) soil organic carbon availability based on a carbon and nitrogen dynamics module (CNDM) (Zhuang et al., 2003); (2) soil temperature profile from a soil thermal module (STM) (Zhuang et al., 2001, 2003); and (3) soil moisture profile from a hydrological module (HM) (Bonan, 1996; Zhuang et al, 2004). Net exchange of CO between the atmosphere and soil is determined by the mass balance approach (net flux = total production – total oxidation – total soil CO concentration change). According to previous studies, we separated active soils (top 30cm) for CO consumption and production into 1 cm thick layers (King, 1999a, 1999b; Whalen & Reeburgh, 2001; Chan & Steudler, 2006). Between the soil layers, the changes of CO concentrations were calculated as:

$$\frac{\partial(C(t,i))}{\partial t} = \frac{\partial}{\partial z}\left(D(t,i)\frac{\partial\big(C(t,i)\big)}{\partial z}\right) + P(t,i) - O(t,i) \qquad (1)$$

Where $C(t,i)$ is the CO concentration in layer i and at time t, units are mg m^{-3}. z is the depth of the soil, units are m. $D(t,i)$ is the diffusion coefficient for layer i, units are $m^2\ s^{-1}$. $P(t,i)$ is the CO production rate and $O(t,i)$ is the CO consumption rate. The units of $P(t,i)$ and $O(t,i)$ are mg $m^{-3}\ s^{-1}$. $D(t,i)$ is calculated using the method from Potter et al. (1996), which are the functions of soil temperature, soil texture and soil moisture. The upper boundary condition is specified as the atmospheric CO concentration, which is estimated by an empirical function of latitude (Potter et al., 1996) or directly measured by the MOPITT satellite during 2000-2013. The lower boundary condition is assumed to have no diffusion exchange with the layer underneath. This partial differential equation (PDE) is solved using the Crank-Nicolson method for less time-step-sensitive solution.

CO consumption was modeled in unsaturated soil pores as:

$$O(t,i) = V_{max} \cdot f_1\big(C(t,i)\big) \cdot f_2\big(T(t,i)\big) \cdot f_3\big(M(t,i)\big) \qquad (2)$$

Where V_{max} is the ecosystem specific maximum oxidation rate and was estimated previously ranging from 0.3 to 11.1 μg CO $g^{-1}\ h^{-1}$ for different ecosystems (Whalen & Reeburgh, 2001). f_i represents the effects of soil CO concentration $C(t,i)$, temperature $T(t,i)$ and moisture $M(t,i)$ on CO soil consumption. Considering CO consumption as the result of microbial activities, we calculated $f_1\big(C(t,i)\big)$, $f_2\big(T(t,i)\big)$ and $f_3\big(M(t,i)\big)$ in a similar way as Zhuang et al. (2004):

$$f_1\big(C(t,i)\big) = \frac{C(t,i)}{C(t,i) + k_{CO}} \qquad (2.1)$$

$$f_2\big(T(t,i)\big) = Q_{10}^{\frac{T(t,i)-T_{ref}}{10}} \qquad (2.2)$$

$$f_3\big(M(t,i)\big) = \frac{(M(t,i) - M_{min})(M(t,i) - M_{max})}{(M(t,i) - M_{min})(M(t,i) - M_{max}) - (M(t,i) - M_{opt})^2} \qquad (2.3)$$

Where $f_1\big(C(t,i)\big)$ is a multiplier that enhances oxidation rate with increasing soil CO concentrations using a Michaelis-Menten function with a half-saturation constant k_{CO}, and their values were previous estimated ranging from 5 to 51 µl CO l^{-1} for different ecosystems (Whalen & Reeburgh, 2001); $f_2\big(T(t,i)\big)$ is a multiplier that enhances CO oxidation rates with increasing soil temperature using a Q10 function with Q_{10} coefficients (Whalen & Reeburgh, 2001). T_{ref} is the reference temperature, units are °C (Zhuang et al., 2004, 2013). $f_3\big(M(t,i)\big)$ is a multiplier to estimate the biological limiting effect that diminishes CO oxidation rates if the soil moisture is not at an optimum level (M_{opt}). M_{min}, M_{max} and M_{opt} are the minimum, maximum and optimum volumetric soil moistures of oxidation reaction, respectively. Equation (2.2) will overestimate CO consumption at higher temperature because in reality CO consumption will decrease at higher temperatures than optimum temperature, while f_2 will keep increasing with rising temperature. However, the CO consumption is constrained by CO production, and equation (1) is used to represent this constraint.

We modeled the CO production rate ($P(t,i)$) as a process of chemical oxidation constrained by soil organic carbon (SOC) decay (Conrad and Seiler,1985; Potter et al. 1996; Jobbagy & Jackson, 2000; van Asperen et al., 2015):

$$P(t,i) = P_r(t,i) \cdot E_{SOC} \cdot C_{SOC}(t) \cdot F_{SOC} \qquad (3)$$

Where $P_r(t,i)$ is a reference soil CO production rate which has been normalized to rate at reference temperature (production rate at temperature (t,i) divided by production rate at reference temperature), which is affected by soil moisture and soil temperature (Conrad and Seiler,1985; van Asperen et al., 2015). E_{SOC} is an estimated nominal CO production factor of 3.5 ± 0.9 X 10^{-9} mg CO m^{-2} s^{-1} per g SOC m^{-2} (to 30 cm surface soil depth) (Potter et al., 1996). $C_{SOC}(t)$ is a SOC content in mg m^{-2}, which is provided by

CNDM module in TEM. F_{SOC} is a constant fraction of top 30cm SOC compared to total amount of SOC, which is 0.33 for shrubland areas, 0.42 for grassland areas and 0.50 for forest areas, respectively (Jobbagy & Jackson, 2000). $P_r(t,i)$ was calculated as:

$$P_r(t,i) = \exp\left(f_4\big(M(t,i)\big) \cdot Ea_{ref}/R \cdot \left(\frac{1}{273.15 + PT_{ref}} - \frac{1}{T(t,i) + 273.15}\right)\right) \quad (3.1)$$

$$f_4\big(M(t,i)\big) = \frac{PM_{ref}}{M(t,i) + PM_{ref}} \quad (3.2)$$

Where equation (3.1) is derived from Arrhenius equation for chemical reactions and normalized using the reference temperature PT_{ref}. Ea_{ref}/R is the reference activation energy divided by gas constant R, units are K. $f_4\big(M(t,i)\big)$ is the multiplier that reduces activation energy using a regression approach based on laboratory experiment of moisture influences on CO production (Conrad and Seiler,1985). PM_{ref} is the reference volumetric soil moisture, ranging from 0.01 to 0.5 volume/volume (v/v). We assumed thermal-degradation as the main CO producing process due to lack of photo-degradation data and hard to distinguish photo-degradation from observations. In order to reduce the bias from thermal-degradation to total abiotic degradation, the equation (3.1) is parameterized by comparing with total production rate. For instance, $P_r(t,i)$ calculation can perfectly fit the experiment results in Van Asperen et al., 2015 with proper PT_{ref}(18°C), Ea_{ref}/R(14000 K) and PM_{ref}(0.5 v/v).

CO deposition velocity was modeled in the same way as equation (19.1) in Seinfeld, et al. (1998):

$$v_d = -F_{net}/C_{CO,air} \quad (4)$$

Where the v_d is the CO deposition velocity, units are mm s^{-1}; F_{net} is the model estimated CO net flux rate, units are mg CO m^{-2} day^{-1}; $C_{CO,air}$ is the CO surface concentration, units are ppbv. $C_{CO,air}$ can be MOPITT CO surface concentration data or derived CO surface concentrations using the same method as Potter et al. (1996). Positive values of v_d are soil uptake (deposition from air to soils) and negative values are soil emission.

2.3 Model Parameterization and Extrapolation

The model parameterization was conducted in two steps: 1) Thermal and hydrology modules embedded in TEM were revised, calibrated and evaluated by running model with corresponding local meteorological or climatic data at four representative sites, including boreal forest, temperate forest, tropical forest and savanna (Table 1, site No.1 to 4, Figure 2) to minimize model data mismatch in terms of soil temperature and moisture. 2) CODM module was parameterized by running TEM for observational periods with the corresponding local meteorological or climatic data at each reference site (Table 1, Figure 3), and using the Shuffled Complex Evolution Approach in R language (SCE-UA-R) (Duan et al., 1993) to minimize the difference between simulated and observed net CO flux. Eleven parameters including k_{CO}, V_{max}, T_{ref}, Q_{10}, M_{min}, M_{max}, M_{opt}, E_{SOC}, Ea_{ref}/R, PM_{ref} and PT_{ref} were optimized (Table 2). To be noticed, F_{SOC} was not involved in the calibration process. Parameter priors were decided based on previous studies (Conrad & Seiler, 1985; King, 1999b; Whalen & Reeburgh, 2001; Zhuang et al., 2004). SCE-UA-R was used for site No. 6, 8, 10, 11 (Table 1). Each site has been run 50 times using SCE-UA-R with 10000 maximum loops for parameter ensemble, and all of them reached stable state before the end of the loops. For wetlands, the only available data is from site No.12. We used a trial-and-error method to make our simulated results in the range of observed flux rates, with a 10% tolerance. For tropical sites, since tropical savanna vegetation type is a combination type of tropical forest and grassland in our model, we first used Site No. 13 to set priors to fit the experiment results with a 10% tolerance and then evaluated by running our model comparing with site No.7 results. Site No. 9 and 5 were used to evaluate our model results for temperate forest and grassland. Besides the observed climatic and soil property data, we used ERA-Interim reanalysis data from The European Centre for Medium-Range Weather Forecasts (ECMWF) (Dee et al., 2011), AmeriFlux observed meteorology data (http://ameriflux.lbl.gov/) and reanalysis climatic data from Climatic Research Unit (CRU, Harris et al., 2013) to fill the missing environmental data. To sum up, parameters for various ecosystem types in Table 2 were the final results of our parameterization. Model parameterization was conducted for ecosystem types including boreal forest, temperate coniferous forest, temperate deciduous forest, and grassland using SCE-UA-R. Tropical forest and wet tundra used

a trial-and-error method to adjust parameters letting simulation results best fit the lab data. Due to limited data availability, we assumed temperate evergreen broadleaf forest having the same parameters as temperate deciduous forest.

2.4 Data Organization

To get spatially and temporally explicit estimates of CO consumption, production and net flux at the global scale, we used the data of land cover, soils, climate and leaf area index (LAI) from various sources at a spatial resolution of 0.5° latitude X 0.5° longitude to drive TEM. The land cover data include potential vegetation distribution (Melillo et al., 1993) and soil texture (Zhuang et al., 2003), which were used to assign vegetation- and texture-specific parameters to each grid cell.

For the simulation of the period 1901-2013, monthly air temperature, precipitation, clouds fraction and vapor pressure data sets from CRU were used to estimate the soil temperature, soil moisture and SOC with TEM (Figure 4). Monthly LAI data from TEM were required to simulate soil moisture (Zhuang et al., 2004). During this period time, we used an empirical function of latitude, which was derived from the observed latitudinal distribution of tropospheric carbon monoxide (Badr and Probert, 1994) to calculate static CO surface concentration distribution (equation (7), Potter et al., 1996):

$$C_{CO,air} = 82.267856 + 0.8441503L + 1.55934 \times 10^{-2}L^2 + 2.37 \times 10^{-5}L^3 - 2.3 \times 10^{-6}L^4 \quad (5)$$

Where $C_{CO,air}$ is the derived surface CO concentration (ppbv), L represents latitude which is negative degrees for southern hemisphere and positive degrees for northern hemisphere. We also used the atmospheric CO data from MOPITT satellite during 2000-2013 (Figure 5). We averaged day-time and night-time monthly mean retrieved CO surface level 3 data (variables mapped on 0.5° latitude X 0.5° longitude grid scales with monthly time step, Gille, 2013) to represent the CO surface concentration level in each month. The missing pixels were fixed by the average of pixels which had values and were inside 1.5 times of the distance between this missing pixel and the nearest pixel with values. These global mean values shown in Figure 5 do not include ocean surfaces, thus there are differences between our surface CO

concentration results and Yoon and Pozzer's report in 2014, which is as low as 99.8ppb. From 2014 to 2100, we used Intergovernmental Panel on Climate Change (IPCC) future climate scenarios from Representative Concentration Pathways (RCPs) climate forcing data sets RCP2.6, RCP4.5 and RCP8.5 (Figure 6). RCP2.6, 4.5 and 8.5 datasets are future climate projections with anthropogenic greenhouse gas emission radiative forcing of 2.6 W m^{-2}, 4.5 W m^{-2} and 8.5 W m^{-2}, respectively, by 2100. Since RCPs did not have water vapor pressure data, we used the specific humidity and sea level air pressure from the RCPs and elevation of surface to estimate the monthly surface vapor pressure (Seinfeld & Pandis, 1998).

2.5 Model Experiment Design

We conducted two sets of core simulations and eight sensitivity test simulations for a historical period. The two core sets of simulations were driven with MOPITT CO surface concentrations data for the period 2000-2013 (experiment E1) and with spatially distributed CO surface concentrations assuming as constant over time estimated from an empirical function of latitude for the period 1901-2100 (experiment E2), respectively. Specifically, in experiment E2 we used the CRU climate forcing for the historical period 1901-2013 and the climate data of RCP2.6, RCP4.5 and RCP8.5 for different future scenarios to examine the responses of CO flux to changing climates. Eight sensitivity simulations were driven with varying different forcing variables while keeping others as they were: 1) with constant CO surface concentrations ± 30%, 2) SOC ±5~~30~~%, 3) precipitation ±20% and 4) air temperature ± 3°C for each pixel, respectively, during 1999-2000 (E3).

3. Results

3.1 Site Evaluation

Both the magnitude and variation of the simulated soil temperature and moisture from cold areas to warm areas compared well to the observations (Figure. 2). The magnitude of the simulated CO flux is comparable and correlated with the observations (r is about 0.5, p-value < 0.001, Figures 3, a2, b2, c2, d2). Estimated CO fluxes for

different ecosystem types range from -28.4 to 1.7 mg CO m^{-2} day^{-1}, and the root mean square error (RMSE) between simulation and observation at all sites is below 1.5 mg CO m^{-2} day^{-1}. RMSE for site No. 7 is bigger than 2.0 mg CO m^{-2} day^{-1} when compared with transparent chamber observations. For boreal forest site, we only had 8 acceptable points in 1994 and 1996 (Figure 3c2).

3.2 Global Soil CO Dynamics During 2000-2013

Using the MOPITT CO surface concentration data during 2000-2013 (E1), the estimated mean soil CO consumption, production and net flux (positive values indicate CO emissions from soils to the atmosphere) are from -197 to -180, 34 to 36 and -163 to -145 Tg CO yr^{-1}, respectively (Figure 7a). Consumption is about 4 times larger than production. The annual consumption and net flux trends follow the atmospheric CO concentration trends (Figure 5b, Figure 7a), with a small interannual variability (<10%). The latitudinal distributions of consumption, production and net fluxes share the same spatial pattern. Around 20°S-20°N and 20-60N° are the largest and second largest areas for production and consumption, while the 45°S-45°N area accounts for nearly 90% of the total consumption and production (Figure 7b, Table 3). The Southern and Northern Hemispheres have 41% and 59% of the total consumption, and 47% and 53% of the total production, respectively (Table 3). The highest rates of consumption and production are located in areas close to the equator, and consumption from areas such as eastern US, Europe and eastern Asia also is high (>-1000 mg m^{-2} yr^{-1}) (Figure 8a, b). Global soils serve as an atmospheric CO sink (Figure 8c). Some areas, such as western US and southern Australia, are CO sources, all of which are grasslands or experiencing dry climate. Tropical evergreen forests are the largest sinks, consuming 86 Tg CO yr^{-1}, and tropical savanna and deciduous forest are second and third largest sinks, consuming a total of 37 Tg CO yr^{-1} (Table 4). These three ecosystems account for 66% of the total consumption. Tropical evergreen forests are also the largest source of soil CO production, producing 16 Tg CO yr^{-1}, while tropical savanna has a considerable production of 6 Tg CO yr^{-1} (Table 4). Moreover, tropical areas, including forested wetlands, forested floodplain and evergreen forests, are most efficient for CO consumption, ranging from -18 to -13 mg CO m^{-2} $day^{-1.}$ They are also the most efficient

for CO production at over 2 mg CO m^{-2} day^{-1} (Table 4, calculated by fluxes divided by area).

3.3 Global Soil CO Dynamics During 1901-2100

Using the constant CO surface concentration, the estimated global mean CO deposition velocities are 0.16-0.19 mm s^{-1} for the period 1901-2013. For the period 2014-2100, deposition velocities are 0.18-0.21, 0.18-0.24 and 0.17-0.31 for RCP2.6, 4.5 and 8.5 scenarios, respectively (Figure 9). During 2014-2100, there are significant trends of increasing deposition velocities for nearly all scenarios (Figure 9). The rates of increasing are 0.0002, 0.0005 and 0.0013 mm s^{-1} yr^{-1}, and will reach 0.20, 0.23 and 0.30 mm s^{-1} by the end of the 21st century for the RCP2.6, RCP4.5 and RCP8.5 scenarios, respectively (Figure 9). These increasing trends are similar to air temperature increasing trends (Figure 6a). Global distribution patterns of CO deposition velocity are similar to net flux distribution for the period 2000-2013 but there are significant differences among 1901-2013, RCP2.6, RCP4.5 and RCP8.5 scenarios (Figure 10). Deposition velocities are increasing from RCP2.6 to RCP8.5 and larger than in the historical periods in areas near the equator (Figure 10). Areas near the equator and eastern Asia become big sinks of atmospheric CO, while northeastern US becomes a small source in the 21st century (Figure 10). Different vegetation types have a large range of deposition velocity, from 0.008 to 1.154 mm s^{-1} (Table 4). The tropical forested wetland, tropical forested floodplain and tropical evergreen forest have top three largest deposition velocity of 1.154, 1.117 and 0.879 mm s^{-1}, respectively, while desert, short grasslands, and wet tundra have the smallest deposition velocity 0.008, 0.010 and 0.015 mm s^{-1}, respectively.

3.4 Sensitivity test

Eight sensitivity tests have been conducted for the 1999-2000 period, including changing atmospheric CO by ±30%, SOC by ±5~~30~~%, precipitation by ±30% and air temperature by ±3°C for each pixel (Table 5). Soil CO consumption is most sensitive

(changing 29%) to air temperature while production is most sensitive ~~(changing up to 36%)~~ to both air temperature (changing up to 36%) and SOC (~~5~~30%). The net CO fluxes have the similar sensitivities as consumption. Annual CO consumption, production and net flux follow the change of air temperature (Table 5). In addition, a 30% change in precipitation will not lead to large changes in CO flux (< 3%).

4. Discussion

4.1 Comparison with Other Studies

Previous studies estimated a large range of global CO consumption from -16 to -640 Tg CO yr^{-1}. Our estimates are from -197 to -180 Tg CO yr^{-1} for for 2000-2013 using MOPITT satellite CO surface concentration data. Previous studies also provided a large range for CO production from 0 to 7.6 mg m^{-2} day^{-1} (reviewed in Pihlatie et al., 2016). Our results showed averaged CO production ranging from 0.01 to 2.29 mg m^{-2} day^{-1}. Previously reported CO deposition velocities for different vegetation types range from 0.0 to 4.0 mm s^{-1} while our results showed an averaged CO deposition velocity ranging from 0.006 to 1.154 mm s^{-1} for different vegetation types. The large uncertainty of these estimates is mainly due to a different consideration of the microbial activities, the depth of the soil, and the parameters in the model. In contrast to the estimates of -57 to -16 Tg CO yr^{-1} which were based on top 5 cm soils (Potter et al., 1996), our estimates considered 30cm soils, just as used in Whalen & Reeburgh (2001). In addition, we used a thinner layer division (1cm each layer) for diffusion process, and used the Crank-Nicolson method to solve partial differential equations to avoid time step influences. We also included the microbial CO oxidation process to remove the CO from soils and the effects of soil moisture, soil temperature, vegetation type and soil CO substrate on microbial activities. Our soil thermal, soil hydrology and carbon and nitrogen dynamics simulated in TEM provided carbon substrate spatially and temporally for estimating soil CO dynamics. Overall, although a few previous studies have examined the long-term impacts of climate, land use and nitrogen depositions on CO dynamics (Chan &

Steudler, 2006, Pihlatie et al., 2016), the global prediction of soil CO dynamics still has a large uncertainty.

4.2 Major Controls to Soil CO Dynamics

Sensitivity tests indicate that consumption is normally much larger than CO production so that the former will determine the dynamics of the net flux (Table 5). Model being sensitive to air temperature explains the small increasing trends after the 1960s, the significant increasing trend in the 21st century and the large sinks over tropical areas (Table 5, Figure 9). SOC did not directly influence CO consumption. For instance, increasing SOC led to an increase in soil CO substrate, implying that more CO in soils can be consumed. To be noticed, an extra 3~~18~~ Tg CO yr^{-1} was taken up from the atmosphere to soils in sensitivity test when SOC increasing by 5~~30~~% (Table 5), which will be discussed in detail in Section 4.3. CO surface concentrations will only influence the uptake rate and soil CO substrate concentrations, thus influencing the soil CO consumption rate.

Annual CO consumption and net flux have a similar correlation coefficient with forcing variables and both are significantly correlated with air temperature, soil temperature SOC and atmospheric CO concentration ($R > 0.91$ globally, Table 6). Increasing temperature will increase microbial activities, while more SOC will increase soil CO substrate level. Annual CO consumption and net flux have low correlations with annual precipitation and soil moisture, especially at 45°N-45°S ($R<0.54$ Table 6). Annual CO production is strongly correlated with annual mean SOC, air temperature and soil temperature ($R>0.91$), while is less correlated with precipitation, soil moisture and atmospheric CO concentration. Meanwhile, the monthly CO consumption, production and net flux are well correlated with air temperature, soil temperature, precipitation, and soil moisture ($R>0.69$ globally Table 6). The soil moisture is significantly influenced by temperature at a monthly time step since increasing temperature would induce higher evapotranspiration. Monthly CO consumption, production and net flux have low correlations with SOC because it will not change greatly within a month.

The R between annual soil CO consumption and atmospheric CO concentration is 0.91 at the global scale because the atmospheric CO concentration, air temperature, and soil temperature dominate the annual consumption rate. At monthly scale, this R is -0.48 because global atmospheric CO concentrations are high in winter and low in summer while the simulated soil CO consumption shows an opposite monthly variation (Table 6, Figure 11), suggesting that other factors such as precipitation, air temperature, and soil temperature are major controls for monthly CO fluxes.

4.3. Model Uncertainties and Limitations

There are a number of limitations, contributing to our simulation uncertainties. First, due to lacking long-period observational data of CO flux and associated environmental factors, the model parameterization can only be conducted for 4 ecosystem types including boreal forest, temperate coniferous forest, temperate deciduous forest and grassland. Tropical forest calibration is only conducted using a very limited amount of lab experiment data, but tropical areas are hotspots for CO soil-atmosphere exchanges. Besides, tropical forest SOC for top 30cm can be really high according to observations. TEM model may underestimate the top 30cm SOC, which will underestimate production rates, especially in tropical regions. Tropical regions typically have high temperature during the whole year, which may result in overestimation of CO consumption using equation (2.2). The large deviation for tropical savanna (which is mosaic of tropical forest and grassland ecosystems) may be due to using outside air temperature to represent inside air temperature of transparent chamber observations (Varella et al., 2004), and uncertain tropical forest parameterization. Second, we used the conclusion from van Asperen et al. (2015) and only considered the thermal-degradation process for CO production in this study. Photo-degradation process and biological formation process were not considered due to lacking understanding of these processes. Third, the static CO surface concentration derived from the empirical function is lower than MOPITT CO surface concentration, which will lead to underestimation of CO deposition velocity during 1901-2100. Fourth, from sensitivity test (Table 5) we notice that SOC increasing (5%) resulted in a net flux increase (2.57%). The SOC increase enhanced CO production (Equation 3), CO

concentrations (Equation 1), and CO oxidation (Equation 2). When the change of total oxidation is larger than the difference between the change of total production and the change of total soil CO concentration (Equation 1), the estimate of the net flux change is negative (from atmosphere to soil) using a mass balance approach (Section 2.2), leading to a 2.57% increase in net flux in our SOC sensitive test. This is due to the fact that CO production (Equation 3) is calculated independently from oxidation calculation (Equation 2). This will not influence our other results since SOC varies slightly during our simulation periods with only a 3% increase from 1900 to 2013 (Figure 4d) and up to a 4% increase from 2014 to 2100 (Figure 6g). This artifact problem in SOC sensitivity test can be alleviated using a very fine time step (e.g., 1 second), because CO concentrations will change slightly within the short time, allowing net flux roughly equals the difference between production and oxidation within the short time step. If the change of production is bigger than the change of oxidation, the change of net flux will be positive, leading to a decrease of deposit to soil. The downside is that running the model at one second time step will require significantly high computing time.~~Fourth, from sensitivity test (Table 5) and model test (Table 7), we notice that the diffusion and consumption in the model is very sensitive to sudden 30% SOC changes with 5-minute time step. In reality, diffusion and consumption shall only be slightly influenced by indirect changes of soil CO concentration due to SOC changes. When we used 3-minute or 1-minute time step, the model responses to SOC changes are reasonable (Table 7). However, we believe 5-minute step is suitable in this study since SOC varies slightly during the whole global simulation period with only 3% increasing from 1900 to 2013 (Figure 4d) and up to a 4% increase from 2014 to 2100 (Figure 6g). Our model test showed there are small responses to these small amounts of SOC increasing (Table 7).~~ Fifth, our model structure still has a large potential to improve. In this study we divided the top 30cm soil into 30 layers (layer thickness dz=1cm), but finer division will increase the accuracy (Figure 12). We chose dz=1cm because if dz>1cm, the model vertical CO concentration profile will deviate from reality and diffusion process will be influenced significantly. If dz<1cm, it will need much more computing time but don't have much improvement compared to dz=1cm (Figure 12a-e). We notice that the 30-layer division well represents soil CO concentration profile not only for the days with soil

CO net uptake, but also for the days with CO net emission (Figure 12c, f). Sixth, Michaelis-Menten function (equation 2.1) is used in this model and we notice that k_{CO} is normally much larger than $C(t,i)$ in those days of net soil uptake (over ten times larger, Figure 12). However, we can't simplify equation (2.2) to $f_1\big(C(t,i)\big) = \frac{C(t,i)}{k_{CO}}$ since CO concentrations in soils can be larger than in the atmosphere in the days of net emissions and $C(t,i)$ may be close to k_{CO}, which may lead to overestimation of CO oxidation (Figure 12f). Finally, although we focused on natural ecosystems in this study, land-use change, agriculture activity, and nitrogen deposition also affect the soil CO consumption and production (King, 2002; Chan & Steudler, 2006). For instance, soil CO consumption in agriculture ecosystems is 0 to 9 mg CO m^{-2} day^{-1} in Brazil (King & Hungria, 2002). We used grass land or forest ecosystem to represent agriculture areas in CODM module. Our future study shall include these processes and factors.

5. Conclusions

We analyzed the magnitude, spatial pattern, and the controlling factors of the atmosphere-soil CO exchanges at the global scale for the 20th and 21st centuries using a process-based biogeochemistry model. Major processes include atmospheric CO diffusion into soils, microbial oxidation removal of CO, and CO production through chemical reaction. We found that air temperature and soil temperature play a dominant role in determining annual soil CO consumption and production while precipitation, air temperature, and soil temperature are the major controls for the monthly consumption and production. Atmospheric CO concentrations are important for annual CO consumption. We estimated that the global annual CO consumption, production and net fluxes for 2000-2013 are from -197 to -180, 34 to 36 and -163 to -145 Tg CO yr^{-1}, respectively, when using a MOPITT CO surface concentration data. Tropical evergreen forest, savanna and deciduous forest areas are the largest sinks accounting for 66% of the total CO consumption, while the Northern Hemisphere consumes 59% of the global total. During the 20th century, the estimated CO deposition velocity is 0.16-0.19 mm s^{-1}. The predicted CO deposition velocity will reach 0.20-0.30 mm s^{-1} in the 2090s, primarily because of increasing air temperature. The areas near the equator, eastern Asia,

Europe and eastern US will become the sink hotspots because they have warm and moist soils. This study calls for long-period observations of CO flux for various ecosystem types and projection of atmospheric CO surface concentrations from 1901-2100 to improve future estimates of global soil CO consumption. The effects of land-use change, agriculture activities, nitrogen deposition, photo-degradation and biological formation shall also be considered to improve future quantification of soil CO fluxes.

Acknowledgment

This study is supported through projects funded to Q.Z. by Department of Energy (DE-SC0008092 and DE-SC0007007) and the NSF Division of Information and Intelligent Systems (NSF-1028291). The supercomputing resource is provided by Rosen Center for Advanced Computing at Purdue University. We acknowledge Dr. Stephen C. Whalen made the observational CO flux data available to this study. We are also grateful to University of Tuscia (dep. DIBAF), Italy, and their affiliated members, for their help and the use of their field data.

References:

Badr, O., & Probert, S. D.:Carbon monoxide concentration in the Earth's atmosphere. Applied Energy, doi:10.1016/0306-2619(94)90035-3,1994

Badr, O., & Probert, S. D.: Sinks and environmental impacts for atmospheric carbon monoxide, Applied Energy. doi:10.1016/0306-2619(95)98803-A,1995

Bartholemew, G.W., Alexander, M.: Soils as a sink for atmospheric carbon monoxide, Science 212, 1389-1391, doi:10.1126/science.212.4501.1389, 1981

Bartholomew, G. W., & Alexander, M.: Notes. Microorganisms responsible for the oxidation of carbon monoxide in soil. Environmental Science & Technology. American Chemical Society (ACS), doi:10.1021/es00099a013, 1982

Bender, M., & Conrad, R.: Microbial oxidation of methane, ammonium and carbon monoxide, and turnover of nitrous oxide and nitric oxide in soils, Biogeochemistry, Springer Nature, doi:10.1007/bf00002813, 1994

Bergamaschi, P., Hein, R., Heimann, M., & Crutzen, P. J.: Inverse modeling of the global CO cycle: 1. Inversion of CO mixing ratios, Journal of Geophysical Research: Atmospheres, doi:10.1029/1999jd900818, 2000

Bonan, G.: A Land Surface Model (LSM Version 1.0) for Ecological, Hydrological, and Atmospheric Studies: Technical Description and User's Guide, UCAR/NCAR, doi:10.5065/d6df6p5x, 1996

Bourgeau-Chavez, L.L., Garwood, G.C., Riordan, K., Koziol, B.W., Slawski, J.,: Development of calibration algorithms for selected water content reflectometry probes for burned and nonburned organic soils of Alaska. Int. J. Wildland Fire 19, 961e975, doi:10.1071/wf07175, 2012

Bruhn, D., Albert, K. R., Mikkelsen, T. N., & Ambus, P.: UV-induced carbon monoxide emission from living vegetation. Biogeosciences, Copernicus GmbH, doi:10.5194/bg-10-7877-2013, 2013

Castellanos, P., Marufu, L. T., Doddridge, B. G., Taubman, B. F., Schwab, J. J., Hains, J. C., … Dickerson, R. R.: Ozone, oxides of nitrogen, and carbon monoxide during pollution events over the eastern United States: An evaluation of emissions and vertical mixing, Journal of Geophysical Research Atmospheres, 116(16), doi:10.1029/2010JD014540, 2011

Chan, A. S. K., & Steudler, P. A.: Carbon monoxide uptake kinetics in unamended and long-term nitrogen-amended temperate forest soils. FEMS Microbiology Ecology, 57(3), 343–354, doi:10.1111/j.1574-6941.2006.00127.x, 2006

Conrad, R., & Seiler, W.: Role of Microorganisms in the Consumption and Production of Atmospheric Carbon Monoxide by Soil. Appl. Environ, Microbiol., 40(3), 437–445. Retrieved from http://aem.asm.org/cgi/content/abstract/40/3/437, 1980

Conrad, R., & Seiler, W.: Arid soils as a source of atmospheric carbon monoxide, Geophysical Research Letters, doi:10.1029/gl009i012p01353, 1982

608 Conrad, R., & Seiler, W.: Characteristics of abiological carbon monoxide formation from soil organic
609 matter, humic acids, and phenolic compounds, Environmental Science & Technology, American Chemical
610 Society (ACS), doi:10.1021/es00142a004, 1985
611 Conrad, R., Meyer, O., & Seiler, W.: Role of carboxydobacteria in consumption of atmospheric carbon
612 monoxide by soil, Applied and Environmental Microbiology, 42(2), 211–215, 1981
613 Crutzen, P. J., & Giedel, L. T.: A two-dimensional photochemical model of the atmosphere. 2: The
614 tropospheric budgets of anthropogenic chlorocarbons CO, CH4, CH3Cl and the effect of various NOx
615 sources on tropospheric ozone, J. Geophys. Res., 88(Cll), 6641–6661. doi:10.1029/JC088iC11p06641,
616 1983
617 Crutzen, P.J.: Role of the tropics in atmospheric chemistry, The Geophysiology of Amazonia Vegetation
618 Climate Interaction (Dickinson RE, ed.), pp 107–131. John Wiley, New York, 1987
619 Daniel, J. S., & Solomon, S.: On the climate forcing of carbon monoxide, Journal of Geophysical
620 Research-Atmospheres, 103(D11), 13249–13260. doi:10.1029/98JD00822, 1988
621 Dee, D. P., Uppala, S. M., Simmons, A. J., Berrisford, P., Poli, P., Kobayashi, S., … Vitart, F.: The ERA-
622 Interim reanalysis: configuration and performance of the data assimilation system, Quarterly Journal of
623 the Royal Meteorological Society, doi:10.1002/qj.828, 2011
624 Dentener, F., Drevet, J., Lamarque, J. F., Bey, I., Eickhout, B., Fiore, A. M., … Wild, O.: Nitrogen and
625 sulfur deposition on regional and global scales: A multimodel evaluation, Global Biogeochemical
626 Cycles, 20(4), doi:10.1029/2005GB002672, 2006
627 Derendorp, L., Quist, J. B., Holzinger, R., & Röckmann, T.: Emissions of H2 and CO from leaf litter of
628 Sequoiadendron giganteum, and their dependence on UV radiation and temperature, Atmospheric
629 Environment, 45(39), 7520–7524. doi:10.1016/j.atmosenv.2011.09.044, 2011
630 Duan, Q. Y., Gupta, V. K., & Sorooshian, S.: Shuffled complex evolution approach for effective and
631 efficient global minimization, Journal of Optimization Theory and Applications, 76(3), 501–521.
632 doi:10.1007/BF00939380, 1993
633 Duggin, J. A., & Cataldo, D. A.: The rapid oxidation of atmospheric CO to CO2 by soils, Soil Biology and
634 Biochemistry, 17(4), 469–474, doi:10.1016/0038-0717(85)90011-2, 1985
635 Emmons, L. K., Walters, S., Hess, P. G., Lamarque, J.-F., Pfister, G. G., Fillmore, D., … Kloster, S.:
636 Description and evaluation of the Model for Ozone and Related chemical Tracers, version 4 (MOZART-
637 4), Geoscientific Model Development, 3(1), 43–67. doi:10.5194/gmd-3-43-2010, 2010
638 Fenchel, T., King, G. M., & Blackburn, T. H.: Bacterial biogeochemistry: the ecophysiology of mineral
639 cycling, Bacterial biogeochemistry (p. 307 pp). doi:10.1016/B978-0-12-415836-8.00012-8, 1988
640 Ferenci, T., Strom, T., & Quayle, J. R.: Oxidation of carbon monoxide and methane by Pseudomonas
641 methanica, Journal of General Microbiology, 91(1), 79–91. doi:10.1099/00221287-91-1-79, 1975
642 Fisher, M. E.: Soil-atmosphere Exchange of Carbon Monoxide in Forest Stands Exposed to Elevated and
643 Ambient CO2 (Doctoral dissertation), 2003

644 Fraser, W. T., Blei, E., Fry, S. C., Newman, M. F., Reay, D. S., Smith, K. A., & McLeod, A. R.: Emission of
645 methane, carbon monoxide, carbon dioxide and short-chain hydrocarbons from vegetation foliage under
646 ultraviolet irradiation, Plant, Cell and Environment, 38(5), 980–989. doi:10.1111/pce.12489, 2015
647 Funk, D. W., Pullman, E. R., Peterson, K. M., Crill, P. M., & Billings, W. D.: Influence of water table on
648 carbon dioxide, carbon monoxide, and methane fluxes from Taiga Bog microcosms, Global Biogeochem.
649 Cycles, 8(3), 271–278. doi:10.1029/94gb0122, 1994
650 Galbally, I., Meyer, C. P., Wang, Y. P., & Kirstine, W.: Soil-atmosphere exchange of CH4, CO, N2O and
651 NOx and the effects of land-use change in the semiarid Mallee system in Southeastern Australia, Global
652 Change Biology, 16(9), 2407–2419, doi:10.1111/j.1365-2486.2010.02161.x, 2010
653 Gille, J.: MOPITT Gridded Monthly CO Retrievals (Near and Thermal Infrared Radiances) - Version 6
654 [Data set], NASA Langley Atmospheric Science Data Center. doi:10.5067/TERRA/MOPITT/DATA301,
655 2013
656 Gödde, M., Meuser, K., & Conrad, R.: Hydrogen consumption and carbon monoxide production in soils
657 with different properties, Biology and Fertility of Soils, 32(2), 129–134, doi:10.1007/s003740000226, 2000
658 Guthrie, P. D.: The CH4- CO - OH conundrum: A simple analytic approach, Global Biogeochemical
659 Cycles, doi:10.1029/gb003i004p00287, 1989
660 Hardy, K. R., & King, G. M.: Enrichment of High-Affinity CO Oxidizers in Maine Forest Soil. Applied and
661 Environmental Microbiology, 67(8), 3671–3676, doi:10.1128/AEM.67.8.3671-3676.2001, 2001
662 Harris, I., Jones, P. D., Osborn, T. J., & Lister, D. H.: Updated high-resolution grids of monthly climatic
663 observations - the CRU TS3.10 Dataset, International Journal of Climatology, doi:10.1002/joc.3711, 2013
664 He, H., & He, L.: The role of carbon monoxide signaling in the responses of plants to abiotic
665 stresses, Nitric Oxide : Biology and Chemistry / Official Journal of the Nitric Oxide Society, 42, 40–3.
666 doi:10.1016/j.niox.2014.08.011, 2014
667 Heichel, G. H.: Removal of Carbon Monoxide by Field and Forest Soils1, Journal of Environment Quality,
668 American Society of Agronomy, doi:10.2134/jeq1973.00472425000200040001x, 1973
669 Jobbagy, E. G., & Jackson, R.: The vertical Distribution of soil organic carbon and its relation to climate
670 and vegetation, Ecological Applications, 10:2(April), 423–436, doi:10.2307/2641104, 2000
671 Jones, R. D., & Morita, R. Y.: Carbon monoxide oxidation by chemolithotrophic ammonium
672 oxidizers, Canadian Journal of Microbiology, 29(11), 1545–1551, doi:10.1139/m83-237, 1983
673 Khalil, M. A. ., Pinto, J. ., & Shearer, M.: Atmospheric carbon monoxide, Chemosphere - Global Change
674 Science, Elsevier BV, doi:s1465-9972(99)00053-7,1999
675 Khalil, M. A. K., & Rasmussen, R. A.: The global cycle of carbon monoxide: Trends and mass
676 balance, Chemosphere, 20(1–2), 227–242, doi:10.1016/0045-6535(90)90098-E, 1990
677 King, G. M.: Attributes of Atmospheric Carbon Monoxide Oxidation by Maine Forest Soils, Appl. Environ.
678 Microbiol., 65(12), 5257–5264, 1999

King, G. M.: Characteristics and significance of atmospheric carbon monoxide consumption by soils, Chemosphere, 1, 53–63, doi:10.1016/S1465-9972(99)00021-5, 1999a

King, G. M.: Land use impacts on atmospheric carbon monoxide consumption by soils, Global Biogeochemical Cycles, 14(4), 1161–1172, doi:10.1029/2000GB001272, 2000

King, G. M., & Crosby, H.: Impacts of plant roots on soil CO cycling and soil-atmosphere CO exchange, Global Change Biology, 8(11), 1085–1093, doi:10.1046/j.1365-2486.2002.00545.x, 2002

King, G. M., & Hungria, M.: Soil-atmosphere CO exchanges and microbial biogeochemistry of CO transformations in a Brazilian agricultural ecosystem, Applied and Environmental Microbiology, 68(9), 4480–4485, doi:10.1128/AEM.68.9.4480-4485.2002, 2002

King, G. M., & Weber, C. F.: Distribution, diversity and ecology of aerobic CO-oxidizing bacteria, Nature Reviews, Microbiology, 5(2), 107–18, doi:10.1038/nrmicro1595, 2007

King, J. Y., Brandt, L. A., & Adair, E. C.: Shedding light on plant litter decomposition: advances, implications and new directions in understanding the role of photodegradation, Biogeochemistry, 111(1–3), 57–81, doi:10.1007/s10533-012-9737-9, 2012

Kisselle, K. W., Zepp, R. G., Burke, R. A., De Pinto, A. S., Bustamante, M. M. C., Opsahl, S., … Viana, L. T.: Seasonal soil fluxes of carbon monoxide in burned and unburned Brazilian savannas, Journal of Geophysical Research Atmospheres, 107(20), doi:10.1029/2001JD000638, 2002

Kuhlbusch, T. A., Zepp, R. G., Miller, W. L., & A BURKE, R.: Carbon monoxide fluxes of different soil layers in upland Canadian boreal forests, Tellus B. Informa UK Limited, doi:10.1034/j.1600-0889.1998.t01-3-00003.x, 1998

Lamarque, J. F., Emmons, L. K., Hess, P. G., Kinnison, D. E., Tilmes, S., Vitt, F., … Tyndall, G. K.: CAM-chem: Description and evaluation of interactive atmospheric chemistry in the Community Earth System Model, Geoscientific Model Development, 5(2), 369–411, https://doi.org/10.5194/gmd-5-369-2012, 2012

Lee, H., Rahn, T., & Throop, H.: An accounting of C-based trace gas release during abiotic plant litter degradation, Global Change Biology, 18(3), 1185–1195, doi:10.1111/j.1365-2486.2011.02579.x, 2012

Logan, J. A., Prather, M. J., Wofsy, S. C., & McElroy, M. B.: Tropospheric chemistry - A global perspective, J. Geophys. Res., doi:10.1029/JC086iC08p07210, 1981

Lu, Y., & Khalil, M. A. K.: Methane and carbon monoxide in OH chemistry: The effects of feedbacks and reservoirs generated by the reactive products, Chemosphere. Elsevier BV, doi:10.1016/0045-6535(93)90450-j, 1993

Luo, M., Read, W., Kulawik, S., Worden, J., Livesey, N., Bowman, K., & Herman, R.: Carbon monoxide (CO) vertical profiles derived from joined TES and MLS measurements, Journal of Geophysical Research Atmospheres, 118(18), 10601–10613, doi:10.1002/jgrd.50800, 2013

Moxley, J. M., & Smith, K. A.: Factors affecting utilisation of atmospheric CO by soils, Soil Biology and Biochemistry, 30(1), 65–79, doi:10.1016/S0038-0717(97)00095-3, 1998

714 Myhre, G., Shindell, D., Bréon, F. M., Collins, W., Fuglestvedt, J., Huang, J., ... & Nakajima, T.:
715 Anthropogenic and Natural Radiative Forcing. In: Climate Change 2013: The Physical Science Basis,
716 Contribution of Working Group 1 to the Fifth Assessment Report of the Intergovernmental Panel on
717 Climate Change. Table, 8, 714, 2013
718 Nakai, T., Kim, Y., Busey, R. C., Suzuki, R., Nagai, S., Kobayashi, H., … Ito, A.: Characteristics of
719 evapotranspiration from a permafrost black spruce forest in interior Alaska. Polar Science, 7(2), 136–148.
720 doi:10.1016/j.polar.2013.03.003, 2013
721 Philip, R., & Novick, K.: AmeriFlux US-MMS Morgan Monroe State Forest [Data set]. AmeriFlux; Indiana
722 University, doi:10.17190/AMF/1246080, 2016
723 Pihlatie, M., Rannik, Ü., Haapanala, S., Peltola, O., Shurpali, N., Martikainen, P. J., … Mammarella, I.:
724 Seasonal and diurnal variation in CO fluxes from an agricultural bioenergy crop, Biogeosciences.
725 Copernicus GmbH, doi:10.5194/bg-13-5471-2016, 2016
726 Potter, C. S., Klooster, S. A., & Chatfield, R. B.: Consumption and production of carbon monoxide in soils:
727 A global model analysis of spatial and seasonal variation, Chemosphere, 33(6), 1175–1193,
728 doi:10.1016/0045-6535(96)00254-8, 1996
729 Prather, M., and Ehhalt, D.: Atmospheric chemistry and greenhouse gases. Climate Change, 2001: The
730 Scientific Basis (Houghton JT, Ding Y, Griggs DJ, Noguer M, van der Linden PJ, Dai X, Maskell K &
731 Johnson CA, eds), pp. 239–288, Cambridge University Press, Cambridge, UK, 2001
732 Prather, M., Derwent, R., Ehhalt, D., Fraser, P., Sanheeza, E. and Zhou, X.: Other trace gases and
733 atmospheric chemistry, Climate Change, 1994. Radiative Forcing of Climate Change (Houghton JT, Meira
734 Filho LG, Bruce J, Hoesung Lee BA, Callander E, Haites E, Harris N & Maskell K, eds), pp. 76–126,
735 Cambridge University Press, Cambridge, UK, 1995
736 SALESKA, S. R., DA ROCHA, H. R., HUETE, A. R., NOBRE, A. D., ARTAXO, P. E., & SHIMABUKURO,
737 Y. E.: LBA-ECO CD-32 Flux Tower Network Data Compilation, Brazilian Amazon: 1999-2006, ORNL
738 Distributed Active Archive Center, doi:10.3334/ORNLDAAC/1174, 2013
739 Sanderson, M. G., Collins, W. J., Derwent, R. G., & Johnson, C. E.: Simulation of global hydrogen levels
740 using a Lagrangian three-dimensional model, Journal of Atmospheric Chemistry, 46(1), 15–28,
741 doi:10.1023/A:1024824223232, 2003
742 Sanhueza, E., Dong, Y., Scharffe, D., Lobert, J. M., & Crutzen, P. J.: Carbon monoxide uptake by
743 temperate forest soils: The effects of leaves and humus layers, Tellus, Series B: Chemical and Physical
744 Meteorology, 50(1), 51–58, doi:10.1034/j.1600-0889.1998.00004.x, 1998
745 Schade, G. W., & Crutzen, P. J.: CO emissions from degrading plant matter (II). Estimate of a global
746 source strength, Tellus, Series B: Chemical and Physical Meteorology, 51(5), 909–918,
747 doi:10.1034/j.1600-0889.1999.t01-4-00004.x, 1999
748 Scharffe, D., Hao, W. M., Donoso, L., Crutzen, P. J., & Sanhueza, E.: Soil fluxes and atmospheric
749 concentration of CO and CH4 in the northern part of the Guayana shield, Venezuela, Journal of
750 Geophysical Research-Atmospheres, 95(90), 22475–22480, doi:10.1029/JD095iD13p22475, 1990

751 Seiler, W.: In: Krumbein, W.E. (Ed.), Environmental Biogeochemistry and Geomicrobiology, Methods,
752 Metals and Assessment, vol. 3, Ann Arbor Science, Ann Arbor, MI, pp. 773-810, 1987
753 Seinfeld, J. H., & Pandis, S. N.: Atmospheric Chemistry and Physics: From Air Pollution to Climate
754 Change, Atmospheric Chemistry and Physics from Air Pollution to Climate Change Publisher New York
755 NY Wiley 1998 Physical Description Xxvii 1326 p A WileyInterscience Publication ISBN 0471178152, 51,
756 1–4, doi:10.1080/00139157.1999.10544295, 1998
757 Stein, O., Schultz, M. G., Bouarar, I., Clark, H., Huijnen, V., Gaudel, A., … Clerbaux, C.: On the
758 wintertime low bias of Northern Hemisphere carbon monoxide found in global model
759 simulations, Atmospheric Chemistry and Physics, 14(17), 9295–9316, doi:10.5194/acp-14-9295-2014,
760 2014
761 Stevenson, D. S., Dentener, F. J., Schultz, M. G., Ellingsen, K., van Noije, T. P. C., Wild, O., … Szopa, S.:
762 Multimodel ensemble simulations of present-day and near-future tropospheric ozone, Journal of
763 Geophysical Research Atmospheres, 111(8), doi:10.1029/2005JD006338, 2006
764 Suzuki, R.: AmeriFlux US-Prr Poker Flat Research Range Black Spruce Forest [Data set], AmeriFlux;
765 Japan Agency for Marine-Earth Science and Technology, doi:10.17190/AMF/1246153, 2016
766 Tan, Z., & Zhuang, Q.: An analysis of atmospheric CH4 concentrations from 1984 to 2008 with a single
767 box atmospheric chemistry model, Atmospheric Chemistry and Physics Discussions, Copernicus GmbH,
768 doi:10.5194/acpd-12-30259-2012, 2012
769 Tarr, M. a., Miller, W. L., & Zepp, R. G.: Direct carbon monoxide photoproduction from plant
770 matter, Journal of Geophysical Research, 100, 11403, doi:10.1029/94JD03324, 1995
771 Taylor, J. A., Zimmerman, P. R., & Erickson, D. J.: A 3-D modelling study of the sources and sinks of
772 atmospheric carbon monoxide, Ecological Modelling, 88(1–3), 53–71, doi:10.1016/0304-3800(95)00069-
773 0, 1996
774 van Asperen, H., Warneke, T., Sabbatini, S., Nicolini, G., Papale, D., & Notholt, J.: The role of photo- and
775 thermal degradation for CO₂ and CO fluxes in an arid ecosystem, Biogeosciences,
776 12(13), 4161–4174, doi:10.5194/bg-12-4161-2015, 2015
777 Varella, R. F., Bustamante, M. M. C., Pinto, A. S., Kisselle, K. W., Santos, R. V., Burke, R. A., … Viana, L.
778 T.: Soil fluxes of CO2, CO, NO, and N2O from an old pasture and from native Savanna in
779 Brazil, Ecological Applications, 14(4 SUPPL.), doi:10.1890/01-6014, 2004
780 Vreman, H. J., Wong, R. J., & Stevenson, D. K.: Quantitating carbon monoxide production from heme by
781 vascular plant preparations in vitro, Plant Physiology and Biochemistry, 49(1), 61–68,
782 doi:10.1016/j.plaphy.2010.09.021, 2011
783 Wesely, M. L.: Parameterization of surface resistances to gaseous dry deposition in regional-scale
784 numerical models. Atmospheric Environment (1967), Elsevier BV, doi:10.1016/0004-6981(89)90153-4,
785 1989
786 Wesely, M., & Hicks, B.: A review of the current status of knowledge on dry deposition. Atmospheric
787 Environment, 34, 2261–2282, doi:10.1016/S1352-2310(99)00467-7, 2000

Whalen, S. C., & Reeburgh, W. S.: Carbon monoxide consumption in upland boreal forest soils, Soil Biology and Biochemistry, 33(10), 1329–1338, doi:10.1016/S0038-0717(01)00038-4, 2001

Yonemura, S., Kawashima, S., & Tsuruta, H.: Carbon monoxide, hydrogen, and methane uptake by soils in a temperate arable field and a forest, Journal of Geophysical Research, 105(Dll), 14347, https://doi.org/10.1029/1999JD901156, 2000

Yoon, J., & Pozzer, A.: Model-simulated trend of surface carbon monoxide for the 2001-2010 decade, Atmospheric Chemistry and Physics, 14(19), 10465–10482, doi:10.5194/acp-14-10465-2014, 2014

Zepp, R. G., Miller, W. L., Tarr, M. A., Burke, R. A., & Stocks, B. J.: Soil-atmosphere fluxes of carbon monoxide during early stages of postfire succession in upland Canadian boreal forests, Journal of Geophysical Research-Atmospheres, 102(D24), 29301–29311, doi:10.1029/97jd01326, 1997

Zhuang, Q., McGuire, A. D., Melillo, J. M., Clein, J. S., Dargaville, R. J., Kicklighter, D. W., … Hobbie, J. E.: Carbon cycling in extratropical terrestrial ecosystems of the Northern Hemisphere during the 20th century: A modeling analysis of the influences of soil thermal dynamics, Tellus, Series B: Chemical and Physical Meteorology, 55(3), 751–776, doi:10.1034/j.1600-0889.2003.00060.x, 2003

Zhuang, Q., Melillo, J. M., Kicklighter, D. W., Prinn, R. G., McGuire, A. D., Steudler, P. A., … Hu, S.: Methane fluxes between terrestrial ecosystems and the atmosphere at northern high latitudes during the past century: A retrospective analysis with a process-based biogeochemistry model, Global Biogeochemical Cycles, 18(3), doi:10.1029/2004GB002239, 2004

Zhuang, Q., Melillo, J. M., McGuire, A. D., Kicklighter, D. W., Prinn, R. G., Steudler, P. A., … Hu, S.: Net emissions of CH4 and CO2 in Alaska: Implications for the region's greenhouse gas budget, Ecological Applications, 17(1), 203–212, doi:10.1890/1051-0761(2007)017[0203:NEOCAC]2.0.CO;2, 2007

Zhuang, Q., Romanovsky, V. E., & McGuire, a. D.: Incorporation of a permafrost model into a large-scale ecosystem model: Evaluation of temporal and spatial scaling issues in simulating soil thermal dynamics, Journal of Geophysical Research, 106, 33649, doi:10.1029/2001JD900151, 2001

Zhuang, Q., Chen, M., Xu, K., Tang, J., Saikawa, E., Lu, Y., … McGuire, A. D.: Response of global soil consumption of atmospheric methane to changes in atmospheric climate and nitrogen deposition, Global Biogeochemical Cycles, doi:10.1002/gbc.20057, 2013

Table 1. Model parameterization sites for thermal and hydrology modules (site No. 1-4) and for CODM module (site No. 5-13)

No.	Site Name	Location	Vegetation	Driving Climate	Observed Data	Source and Comments
1	Poker Flat Research Range Black Spruce Forest (US_PRR)	147°29'W/65°7'N	Boreal Evergreen Needle Leaf Forests	Site Observation & ERA Interim	Soil Temperature and Moisutre of 2011-2014	Suzuki (2016)
2	Morgan Monroe State Forest (US_MMS)	86°25W/39°19'N	Temperate Deciduous Broadleaf Forests	Site Observation & ERA Interim	Soil Temperature and Moisutre of 1999-2014	Philip and Novick (2016)
3	Santarem, Tapajos National Forest (STM_K83)	54°56'W/3°3'S	Tropical Moist Forest	Site Observation & ERA Interim	Soil Temperature and Moisutre of 2000-2004	SALESKA et al. (2013)
4	Bananal Island Site (TOC_BAN)	50°08'W/9°49'S	Tropical Forest-Savanna	Site Observation & ERA Interim	Soil Temperature and Moisutre of 2003-2006	SALESKA et al. (2013)
5	Eastern Finland (EF)	27°14E/63°9'N	Boreal Grassland	Site Observation & ERA Interim	CO flux of April-November,2011	Pihlatie et.al. (2016)
6	Viterbo, Italy (VI)	11°55'E/42°22'N	Mediterranean Grassland	Site Observation & ERA Interim	CO flux of August, 2013	van Asperen et al. (2015)
7	Brasilia, Brazil (BB)	47°51'W/15°56'S	Tropical Savanna	Site Observation & CRU	CO flux of October 1999 to July 2001	Varella et al. (2004)
8	Orange County, North Carolina (OC)	79°7'W/35°58'N	Temperate Coniferous Forest	AMF_US-Dk3 2002-2003	CO flux of March 2002 to March 2003	Fisher (2003)
9	Tsukuba Science City, Japan (TSC)	140°7'E/36°01'N	Temperate Mixed Forest	Site Observation & ERA Interim	CO flux of July 1996 to September 1997	Yonemura et. al. (2000)
10	Manitoba, Canada (CBS)	96°44'W/56°09'N	Boreal Pine Forest	Site Observation & AMF_CA-Man	CO flux of June-August, 1994	Kuhlbusch et. al (1998)
11	Scotland, U.K. (SUK)	3°12'W/55°51'N	Temperate Deciduous Forests	ERA Interim 1995	CO flux of 1995	Moxley and Smith (1998)
12	Alaska, USA (AUS)	147°41'W/64°52'N	Boreal wetland	CRU 1991	CO flux of Lab Experiment,1991	Funk et al. (1994)
13	Guayana Shield,Bolivar State,Venezuela (GBV)	62°57'W/7°51'N	Tropical Smideciduous Forest	CRU 1985	CO flux of Lab Experiment,1985	Scharffe et al. (1990)

Table 2. Ecosystem-specific parameters in the CODM module[a]

	Ecosystem Type	k_{CO} $(ul\ CO\ l^{-1})$	$Vmax$ $(ug\ CO\ g^{-1}h^{-1})$	T_{ref} (℃)	$Q10$ $(Unitless)$	M_{min} $(\frac{v}{v})$	M_{max} $(\frac{v}{v})$	M_{opt} $(\frac{v}{v})$	E_{SOC}	F_{SOC} $(\frac{g}{g})$	$\frac{Ea_{ref}}{R}$ (K)	PM_{ref} $(\frac{v}{v})$	PT_{ref} (℃)
1	Alpine Tundra & Polar Desert	36.00	0.78	4.00	1.80	0.10	1.00	0.55	3.00	0.33	7700	0.25	30.00
2	Wet Tundra	36.00	0.70	4.00	1.80	0.25	1.00	0.55	3.00	0.42	7700	0.25	30.00
3	Boreal Forest	27.34	1.18	9.81	1.60	0.15	0.64	0.53	2.98	0.50	8827	0.35	26.99
4	Temperate Coniferous Forest	42.64	2.15	6.90	1.87	0.02	0.96	0.53	2.86	0.50	8404	0.38	31.52
5	Temperate Deciduous Forest	40.16	2.43	8.54	1.51	0.17	0.81	0.51	2.45	0.50	8801	0.35	37.44
6	Grassland	42.41	0.49	11.27	1.65	0.16	0.82	0.51	3.09	0.42	14165	0.24	12.29
7	Xeric Shrublands	8.00	0.30	4.00	1.50	0.10	1.00	0.55	3.00	0.33	7700	0.25	30.00
8	Tropical Forest	45.00	2.00	4.00	1.50	0.10	1.00	0.55	3.80	0.50	14000	0.50	18.00
9	Xeric Woodland	8.00	0.30	4.00	1.50	0.10	1.00	0.55	3.00	0.50	7700	0.25	30.00
10	Temperate Evergreen Broadleaf Forest	40.16	2.43	8.54	1.51	0.17	0.81	0.51	2.45	0.50	8801	0.35	37.44
11	Mediterranean Shrubland	45.00	1.50	4.00	1.50	0.10	1.00	0.55	3.00	0.33	7700	0.25	30.00
**	Largest Potential Value	51.00	11.1	15.00	2.00	0.30	1.00	0.60	3.80	--	15000	0.60	40.00

[a] $k_{CO}$is the half-saturation constant for soil CO concentration; $Vmax$ is the specific maximum CO oxidation rate; $T_{ref}$is the reference temperature to account for soil temperature effects on CO consumption; $Q10$ is the an ecosystem-specific Q10 coefficient to account for soil temperature effects on CO consumption; M_{min}, M_{max}, M_{opt} are the minimum, optimum, and maximum volumetric soil moistures of oxidation reaction to account for soil moisture effects on CO consumption; E_{SOC} is an estimated nominal CO production factor, similar as Potter et al. (1996) (10^{-4} mg CO m^{-2} d^{-1} per g SOC m^{-2}); F_{SOC} is a constant fraction of top 20cm SOC compared to total amount of SOC to account for SOC effects on CO production; Ea_{ref}/R is the is the ecosystem-specific activation energy divided by gas constant to account for the reaction rate of production; PM_{ref} is the reference moisture to account for soil temperature effects on CO production; PT_{ref} is the reference temperature to account for soil temperature effects on CO production

822 **Table 3.** Regional soil CO consumption, net flux and production (Tg CO yr^{-1}) during 2000-2013

	South-45S	45S-0	0-45N	45N-North	Global
Consumption	0.22	75.77	91.66	18.90	186.55
Net flux	0.13	59.34	77.17	14.63	151.27
Production	0.09	16.43	14.49	4.27	35.28

823

824

825 **Table 4.** Annual total soil CO consumption, net flux and production in different ecosystems during 2000-2013
826 (E1) and mean CO deposition velocity in different ecosystems during 1901-2013 (E2)

Vegetation Type	Area (10^6 km^2)	Pixels	Consumption (Tg CO yr^{-1})	Net flux (Tg CO yr^{-1})	Production (Tg CO yr^{-1})	Deposition velocity (mm s^{-1})
Alpine Tundra & Polar Desert	5.28	3580	-0.92	-0.69	0.23	0.023
Wet Tundra	5.24	4212	-1.00	-0.42	0.58	0.015
Boreal Forest	12.47	7578	-7.76	-6.01	1.75	0.070
Forested Boreal Wetland	0.23	130	-0.14	-0.09	0.04	0.109
Boreal Woodland	6.48	4545	-2.48	-1.54	0.94	0.036
Non-Forested Boreal Wetland	0.83	623	-0.35	-0.18	0.17	0.029
Mixed Temperate Forest	5.25	2320	-10.49	-9.98	0.51	0.204
Temperate Coniferous Forest	2.49	1127	-3.51	-3.21	0.30	0.185
Temperate Deciduous Forests	3.65	1666	-5.07	-4.83	0.25	0.151
Temperate Forested Wetland	0.15	60	-0.35	-0.35	0.01	0.281
Tall Grassland	3.63	1567	-1.66	-0.65	1.01	0.021
Short Grassland	4.71	2072	-1.05	-0.27	0.78	0.010
Tropical Savanna	13.85	4666	-21.86	-15.88	5.98	0.234
Xeric Shrubland	14.71	5784	-1.95	-1.64	0.31	0.021
Tropical Evergreen Forest	17.77	5855	-85.90	-69.66	16.24	0.879
Tropical Forested Wetland	0.55	178	-3.59	-3.09	0.50	1.154
Tropical Deciduous Forest	4.69	1606	-14.81	-11.78	3.03	0.532
Xeric Woodland	6.85	2387	-8.48	-7.44	1.04	0.246
Tropical Forested Floodplain	0.15	50	-0.89	-0.77	0.12	1.117
Desert	11.61	4170	-0.62	-0.57	0.05	0.008
Tropical Non-forested Wetland	0.06	19	-0.03	-0.02	0.01	0.067
Tropical Non-forested Floodplain	0.36	120	-0.35	-0.24	0.10	0.083
Temperate Non-Forested Weland	0.34	120	-0.33	-0.20	0.14	0.089
Temperate Forested Floodplain	0.10	48	-0.13	-0.12	0.00	0.197
Temperate Non-forested Floodplain	0.10	45	-0.05	-0.03	0.02	0.050
Wet Savanna	0.16	59	-0.39	-0.32	0.07	0.434
Salt Marsh	0.09	35	-0.05	-0.03	0.03	0.035
Mangroves	0.12	38	-0.49	-0.41	0.08	0.809
Temperate Savannas	6.83	2921	-3.83	-3.22	0.61	0.076
Temperate Evergreen Broadleaf	3.33	1268	-7.17	-6.95	0.22	0.252
Mediterranean Shrubland	1.47	575	-0.86	-0.71	0.16	0.100
Total	133.56	59424	-186.55	-151.27	35.28	--

827
828
829
830
831

Table 5. Sensitivity of global CO consumption, net flux and production (Tg CO yr^{-1}) to changes in atmospheric CO, soil organic carbon (SOC), precipitation (Prec) and air temperature (AT)

	Baseline	CO +30%	CO -30%	SOC +530%	SOC -530%	Prec +30%	Prec -30%	AT +3°C	AT -3°C
Consumption	-147.65	-164.14	-131.12	-152.27~~-175.37~~	-143.03~~119.90~~	-150.72	-143.50	-190.59	-114.83
Change (%)	0.00	11.17	-11.19	3.13~~18.78~~	-3.13~~18.79~~	2.08	-2.81	29.09	-22.23
Net flux	-113.65	-130.15	-97.12	-116.58~~-131.18~~	-110.73~~96.10~~	-116.97	-109.32	-144.23	-89.58
Change (%)	0.00	14.51	-14.54	2.57~~15.42~~	-2.57~~15.44~~	2.92	-3.81	26.90	-21.18
Production	33.99	33.99	33.99	35.69~~44.19~~	32.29~~23.80~~	33.74	34.17	46.36	25.25
Change (%)	0.00	0.00	0.00	5.00~~30.00~~	-5.00~~30.00~~	-0.75	0.53	36.39	-25.72

Formatted: Indent: First line: 0"

Table 6. Correlation coefficients between forcing variables (precipitation (Prec), air temperature (Tair), soil organic carbon (SOC), soil temperature (Tsoil), soil moisture (Msoil) and atmospheric CO (CO air)) and absolute values of consumption, production and net flux for different regions and the globe

		Monthly					Annual				
		North-45°N	45°N-0°	0°-45°S	45°S-South	Global	North-45°N	45°N-0°	0°-45°S	45°S-South	Global
Prec	Consumption	0.91	0.96	0.92	-0.34	0.87	0.65	0.21	0.26	0.13	0.52
	Production	0.91	0.70	0.45	-0.34	0.82	0.63	0.10	0.15	-0.11	0.47
	Net flux	0.91	0.97	0.94	-0.33	0.87	0.65	0.25	0.31	0.32	0.54
Tair	Consumption	0.97	0.98	0.91	0.96	0.95	0.92	0.93	0.88	0.84	0.91
	Production	0.96	0.83	0.72	0.98	0.94	0.92	0.92	0.91	0.95	0.91
	Net Flux	0.97	0.97	0.88	0.90	0.95	0.91	0.92	0.85	0.62	0.91
SOC	Consumption	-0.19	0.07	0.21	-0.01	0.15	0.68	0.90	0.92	0.47	0.92
	Production	-0.19	0.31	0.47	-0.02	0.24	0.72	0.92	0.92	0.50	0.93
	Net Flux	-0.19	0.03	0.14	0.00	0.13	0.67	0.88	0.91	0.38	0.91
Tsoil	Consumption	0.97	0.98	0.92	0.96	0.95	0.94	0.93	0.88	0.85	0.95
	Production	0.97	0.83	0.72	0.98	0.94	0.94	0.92	0.91	0.96	0.95
	Net Flux	0.98	0.97	0.88	0.90	0.95	0.93	0.93	0.86	0.63	0.95
Msoil	Consumption	0.85	0.96	0.92	0.19	0.76	0.03	0.22	0.14	0.26	0.22
	Production	0.85	0.75	0.44	0.14	0.69	-0.02	0.12	0.02	0.05	0.17
	Net Flux	0.84	0.96	0.95	0.25	0.77	0.04	0.26	0.19	0.40	0.24
CO Air	Consumption	-0.66	-0.76	-0.29	0.14	-0.48	0.87	0.88	0.81	0.98	0.91
	Production	-0.70	-0.66	0.08	-0.40	-0.66	-0.36	-0.48	-0.54	-0.44	-0.57
	Net Flux	-0.64	-0.73	-0.35	0.55	-0.41	0.92	0.91	0.88	0.99	0.94

868

869

Table 7. Model test for site No.8 during 2002-2003. Time step is for solving equation (1). SOC increasing represents the percentage of SOC increased in each test. Baseline is the simulation using original time step and SOC input. Differences represent new simulation results minus baseline results.

Time Step	SOC Increasing	Units: mg m^{-2} yr^{-1}	Consumption	Production	Diffusion
5min	0%	Baseline	-1611.5	410.0	-1201.5
5min	30%	Differences	-293.0	123.0	-170.0
3min	30%	Differences	-156.7	123.0	-33.7
1min	30%	Differences	-97.4	123.0	25.6
5min	10%	Differences	-97.7	41.0	-56.7
5min	1%	Differences	-9.8	4.1	-5.7

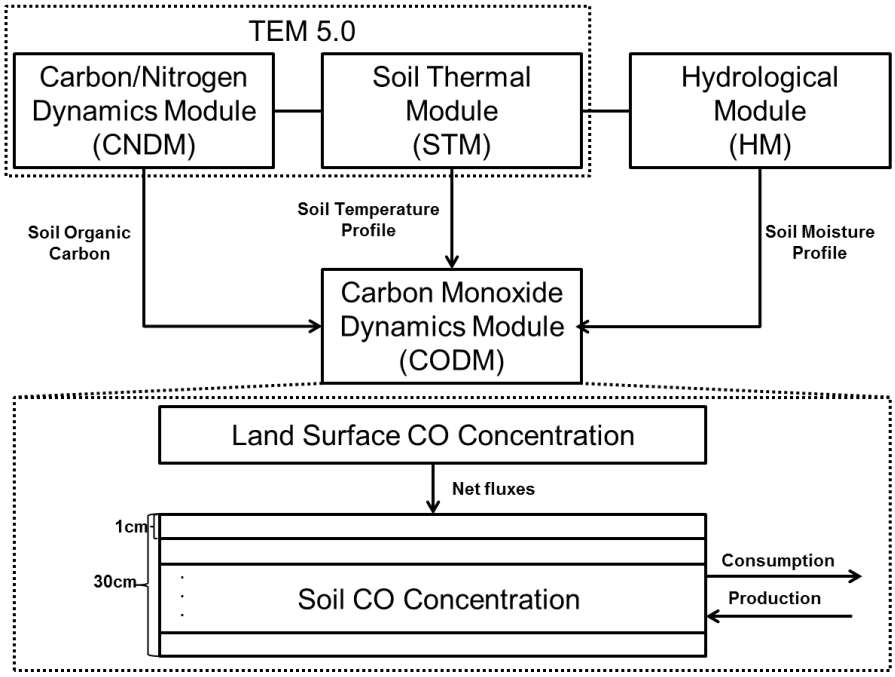

874

875 **Figure 1. The model framework** includes a carbon and nitrogen dynamics module (CNDM), a soil thermal module (STM)
876 from Terrestrial Ecosystem Model (TEM) 5.0 (Zhuang et al., 2001, 2003), a hydrological module (HM) based on a Land
877 Surface Module (Bonan, 1996; Zhuang et al., 2004), and a carbon monoxide dynamics module (CODM). The detailed
878 structure of CODM includes land surface CO concentration as top boundary and thirty 1 cm thick layers (totally 30 cm)
879 where consumption and production take place.

880

881

882

883

884

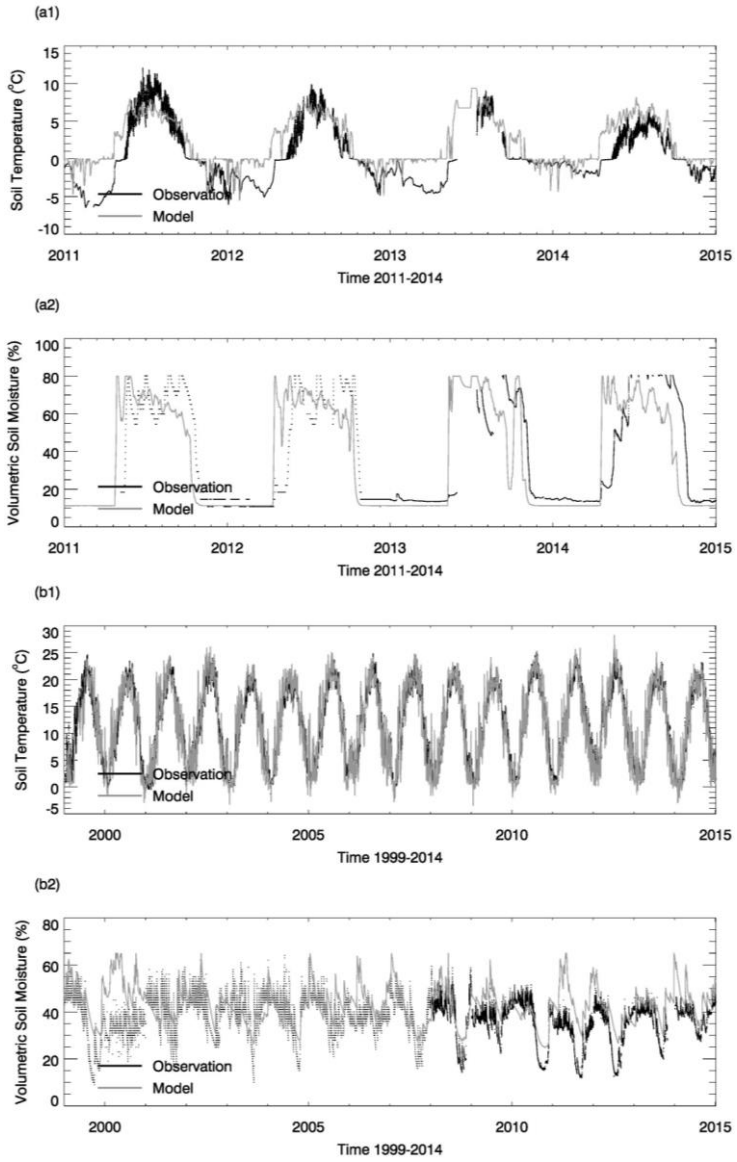

Figure 2. Evaluation of thermal and hydrology module at four sites: (a) Boreal Evergreen Needle Leaf Forests, (b) Temperate Deciduous Broadleaf Forests. (1) shows the soil temperature comparison between model simulations (gray line) and observations (black line) and (2) shows the soil moisture comparison between model simulations (gray line) and observations (black line). Specifically, the volumetric soil moisture is converted from the water content reflectometry (WCR) probe output period using an empirical calibration function of Bourgeau-Chavez et al. (2012) for 5cm-30cm layer. Some of them resulted in calculations of values greater than 100% VSM in Nakai et al. (2013) study. Our model estimated high VSM (close to 80%) is due to top 10 cm moss in the model which has a saturation VSM of 0.8

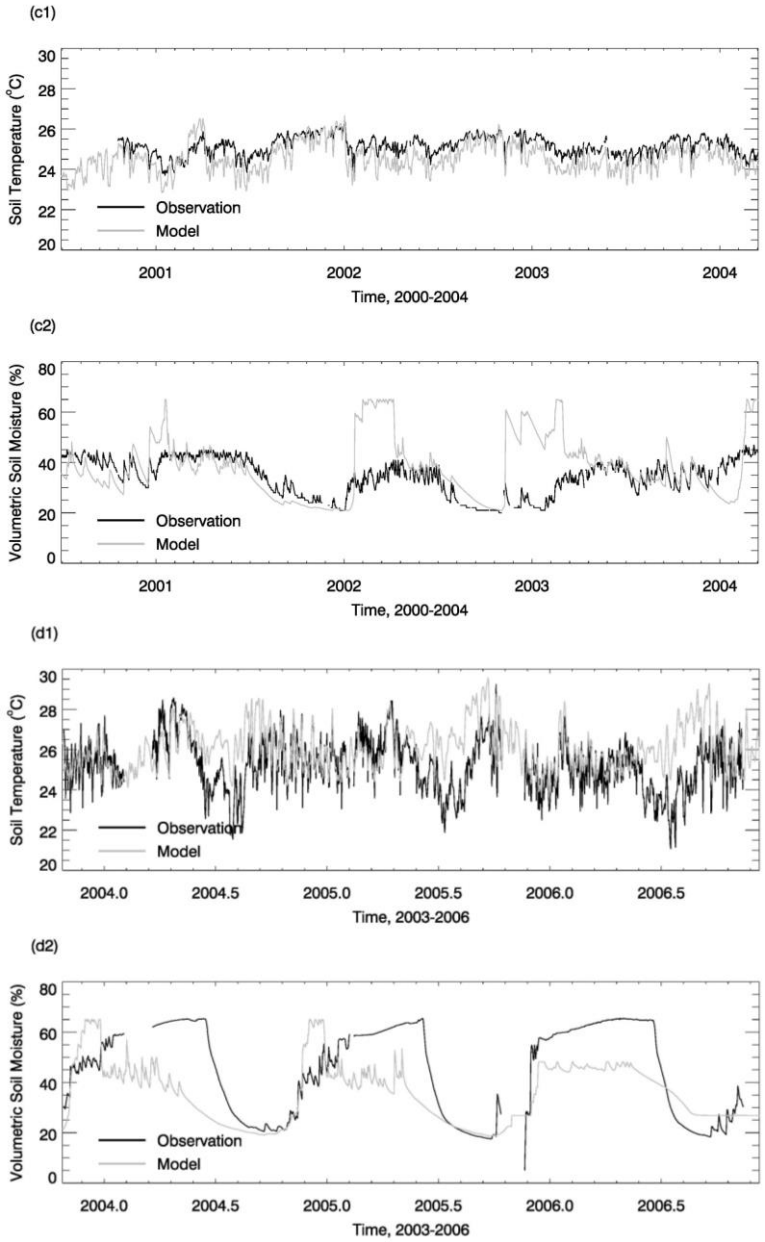

Figure 2. Contd. Evaluation of thermal and hydrology module at four sites: (c) Tropical Moist Forest, (d) Tropical Forest-Savanna. (1) shows the soil temperature comparison between model simulations (gray line) and observations (black line) and (2) shows the soil moisture comparison between model simulations (gray line) and observations (black line)

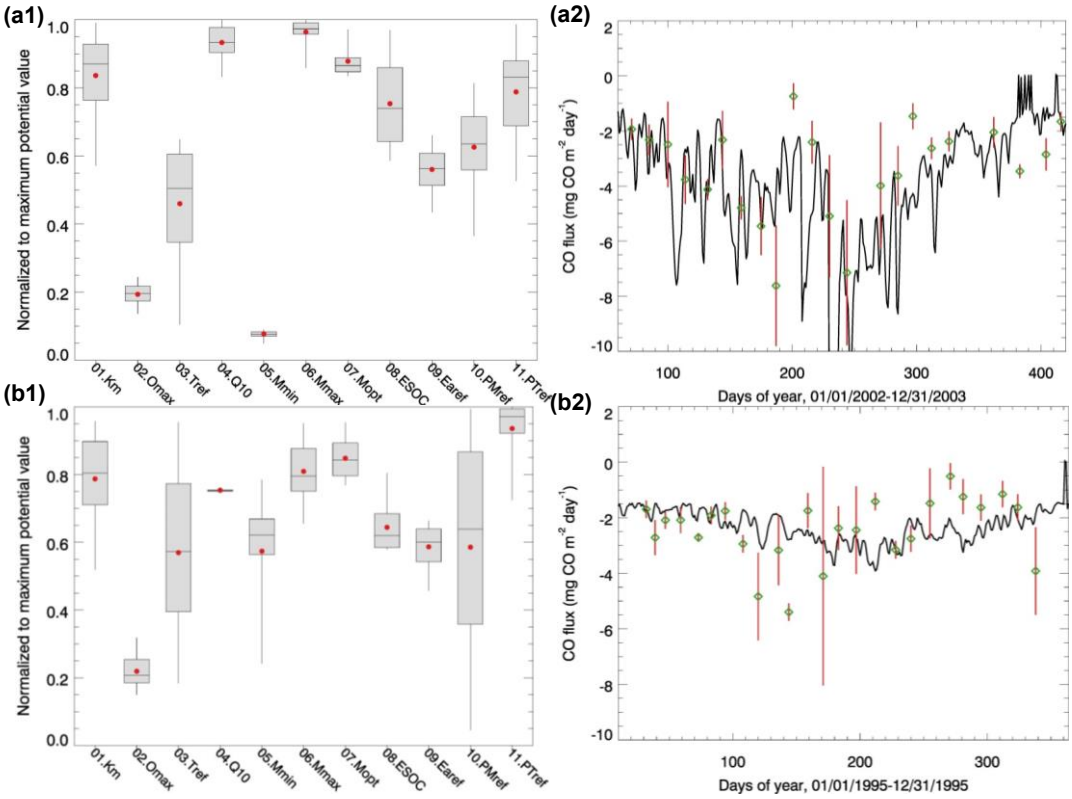

Figure 3. Parameter ensemble experiment results: Each parameter has 50 calibrated values generated from running SCE-UA-R 50 times independently. Parameters are normalized to their largest potential values described in Table 2. (a1) and (a2) are temperate coniferous forest normalized parameter distribution boxplots and CO flux comparisons between model simulations (solid line, using mean value of parameters) and observations (green diamond, red lines represent error bar, site No.8), respectively. For each box, line top, box top, horizontal line inside box, box bottom and line bottom represent maximum, third quartile, median, first quartile and minimum of 50 parameter values. Red dot represents the mean value of 50 parameter values. (b1) and (b2) are plots for temperate deciduous forest (site No.11).

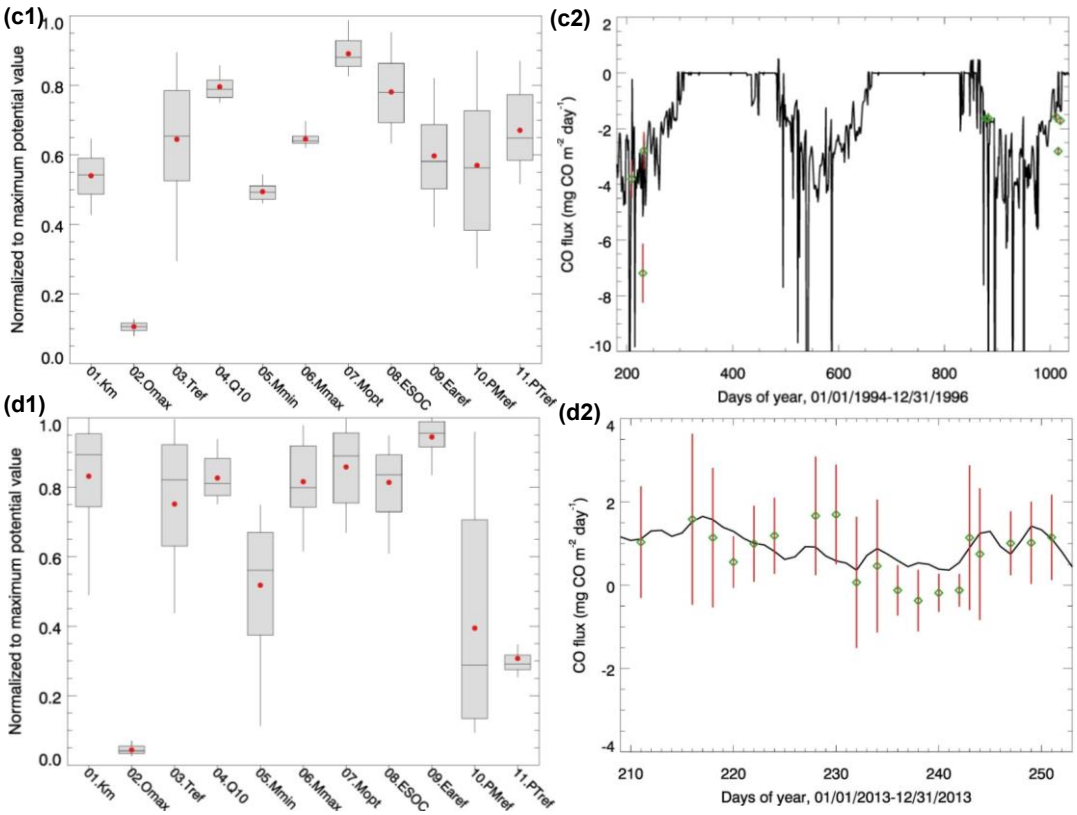

Figure 3. Contd. Parameter ensemble experiment results: Each parameter has 50 calibrated values generated from running SCE-UA-R 50 times independently. Parameters are normalized to their largest potential values described in Table 2. (c1) and (c2) are boreal forest normalized parameter distribution boxplots and CO flux comparisons between model simulations (solid line, using mean value of parameters) and observations (green diamond, red lines represent error bar, site No. 12), respectively. For each box, line top, box top, horizontal line inside box, box bottom and line bottom represent maximum, third quartile, median, first quartile and minimum of 50 parameter values. Red dot represents the mean value of 50 parameter values. (d1) and (d2) are for grassland (site No.6). Grassland observation data is the sum of hourly observations so error bar represented the standard deviation.

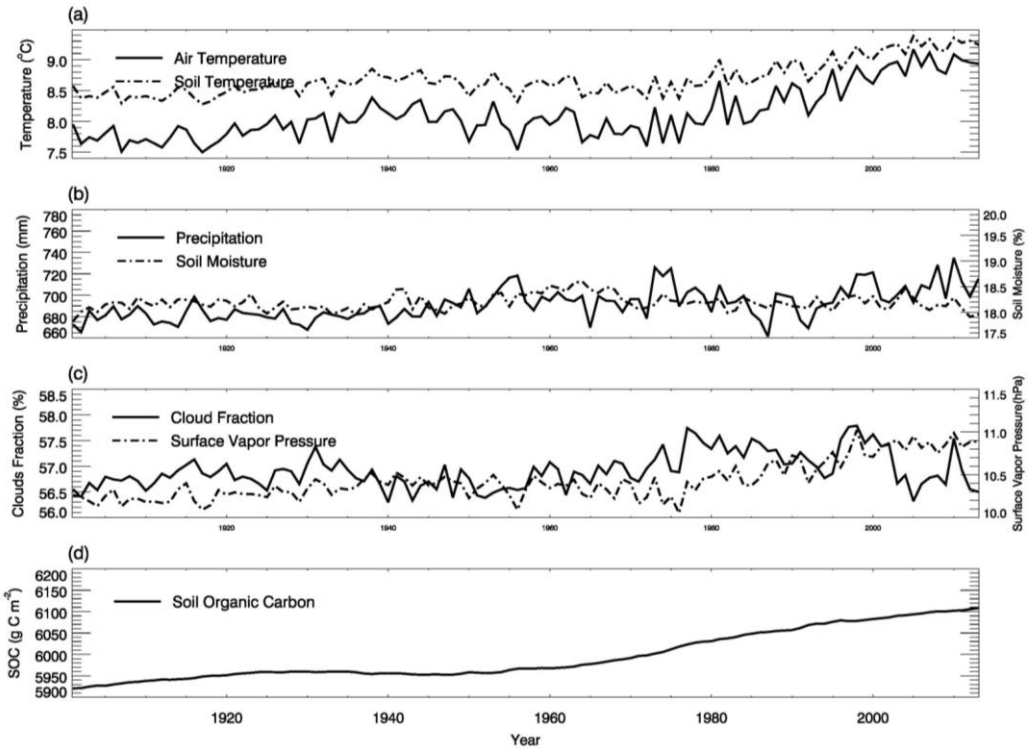

Figure 4. Historical global land surface (excluding Antarctic area and ocean area) mean climate, and simulated global mean soil moisture, soil temperature and SOC for the period 1901-2013.

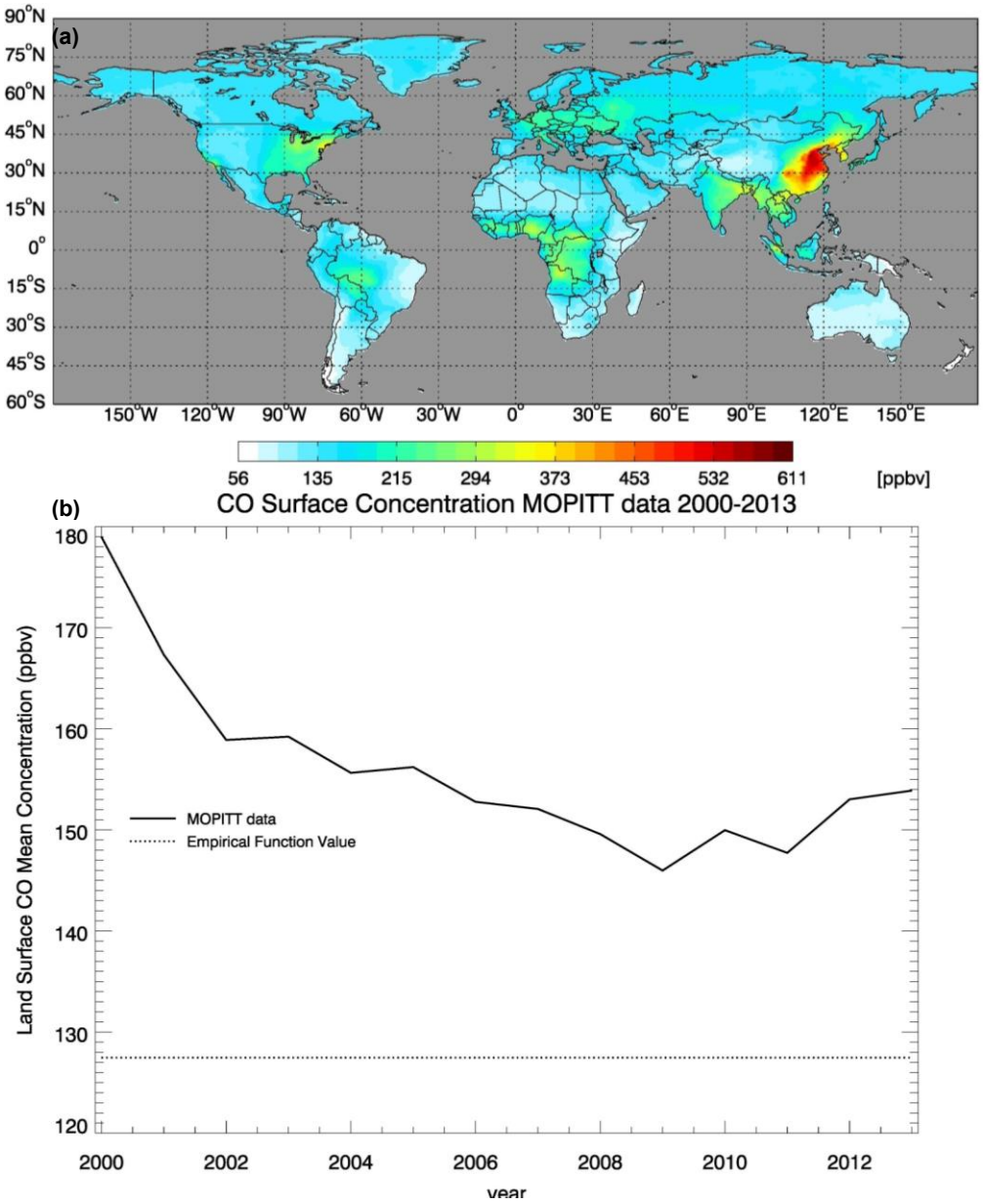

Figure 5. CO surface concentration data from MOPITT satellite (ppbv): (a) global mean CO surface concentrations from MOPITT during 2000-2013; (b) the CO annual surface concentrations from both MOPITT and empirical functions (Potter et al., 1996).

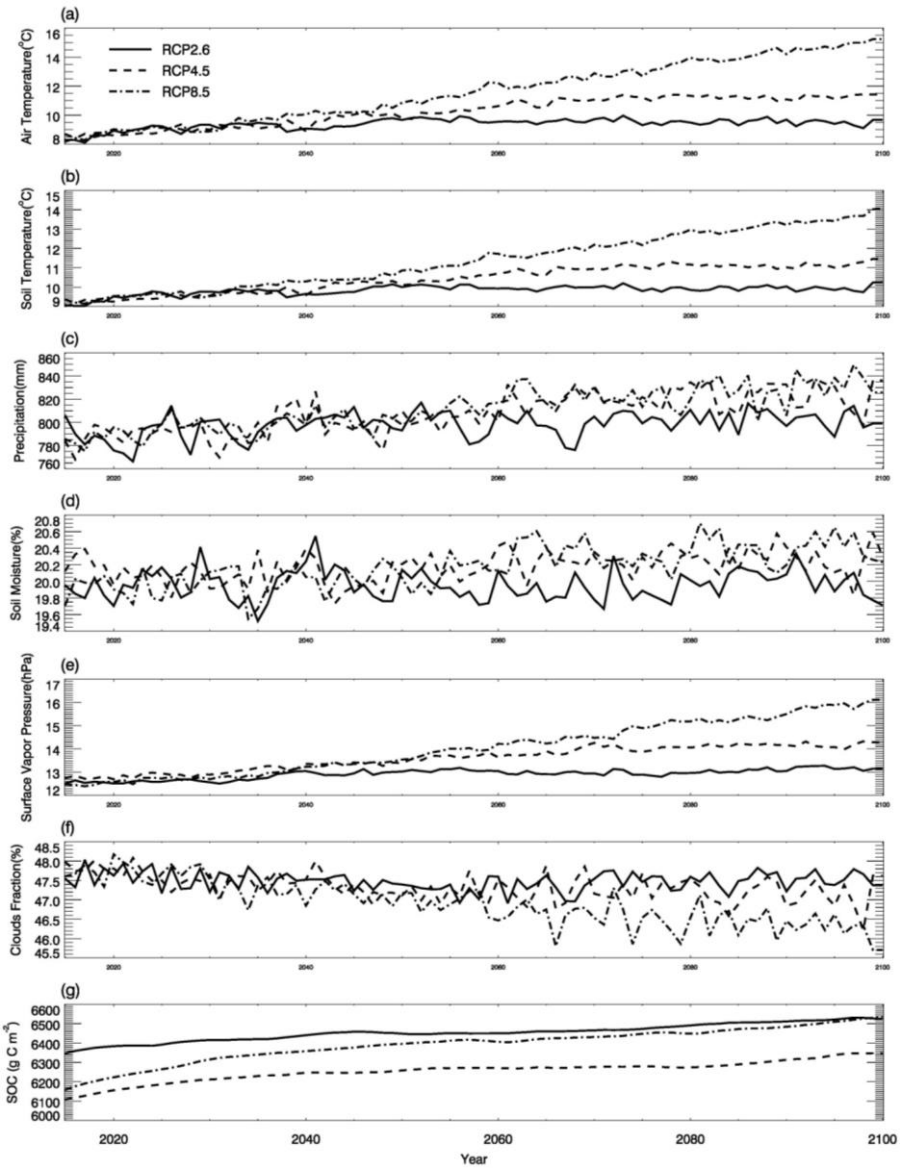

Figure 6. Global land surface (excluding Antarctic area and ocean area) mean climate from RCP2.6, RCP4.5 and RCP8.5 data sets and simulated mean soil temperature, moisture and SOC: (a)-(g) are land surface air temperature (°C), soil temperature (°C), precipitation (mm), soil moisture (%), surface water vapor pressure (hpa), cloud fraction (%), and SOC (mg m^{-2}), respectively.

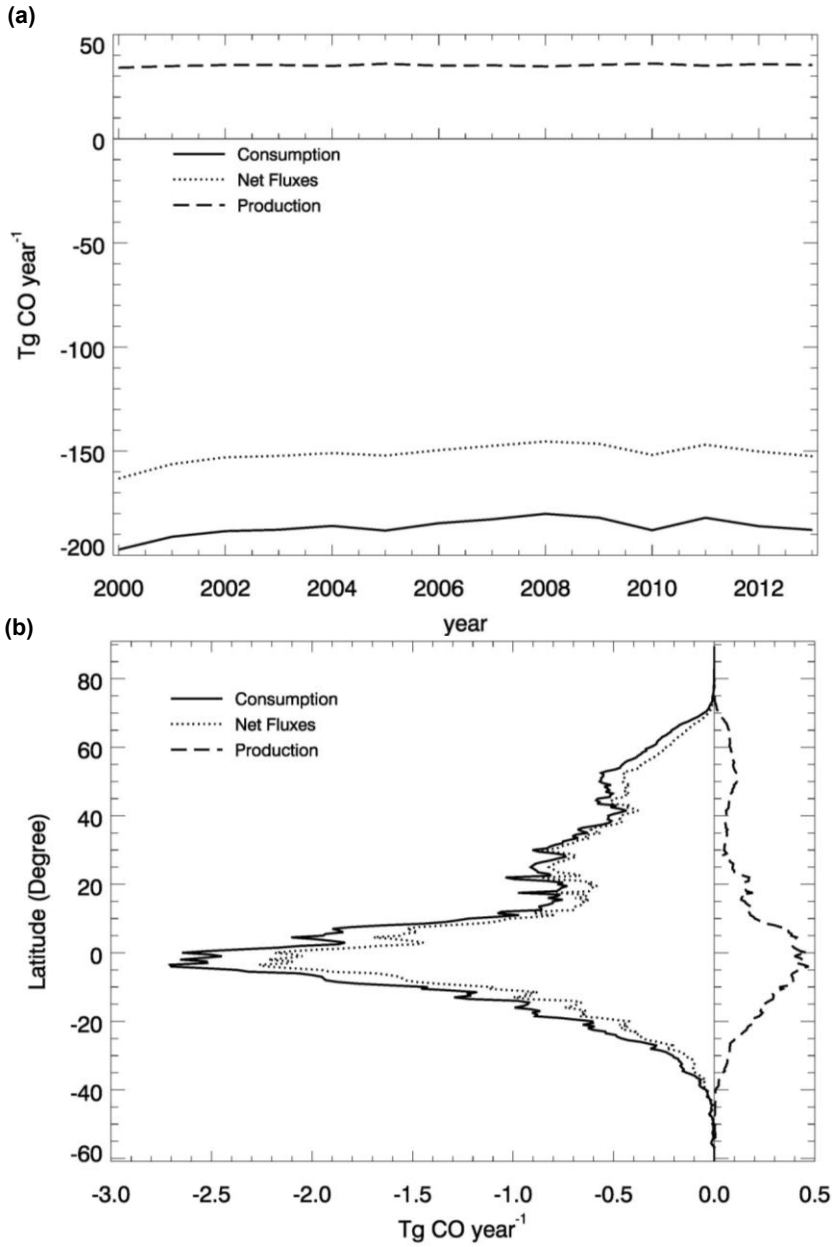

Figure 7. Global mean soil CO consumption, production and net flux: (a) annual time series during 2000-2013and (b) latitudinal distribution during 2000-2013.

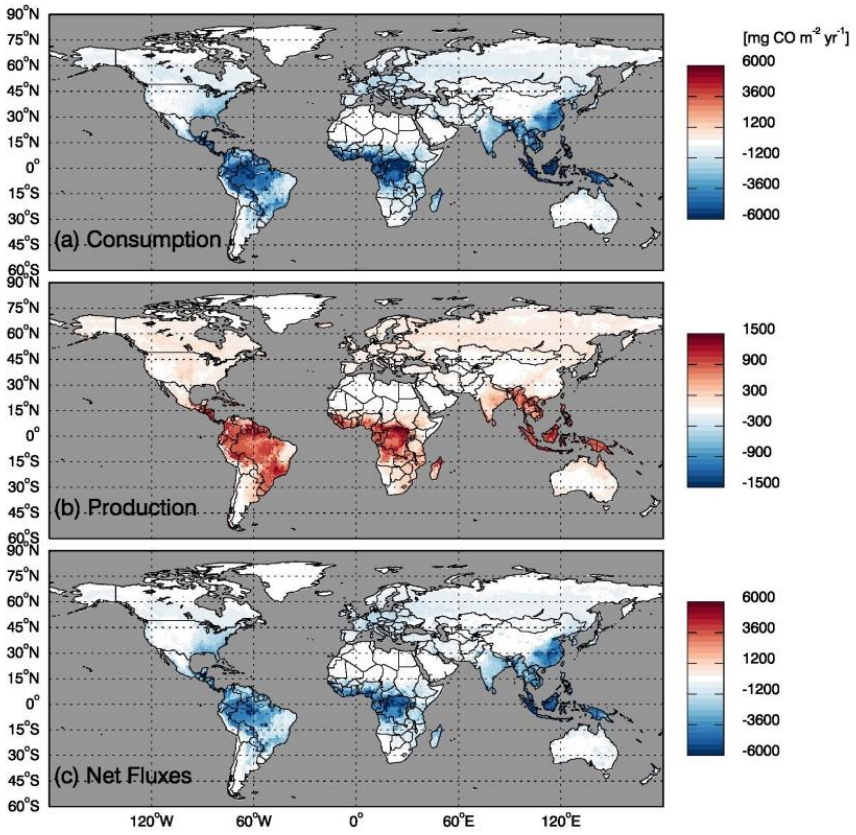

1091

1092

Figure 8. Global annual mean soil CO fluxes (mg CO m^{-2} yr^{-1}) during 2000-2013 using MOPITT CO atmospheric surface concentration data (right side)

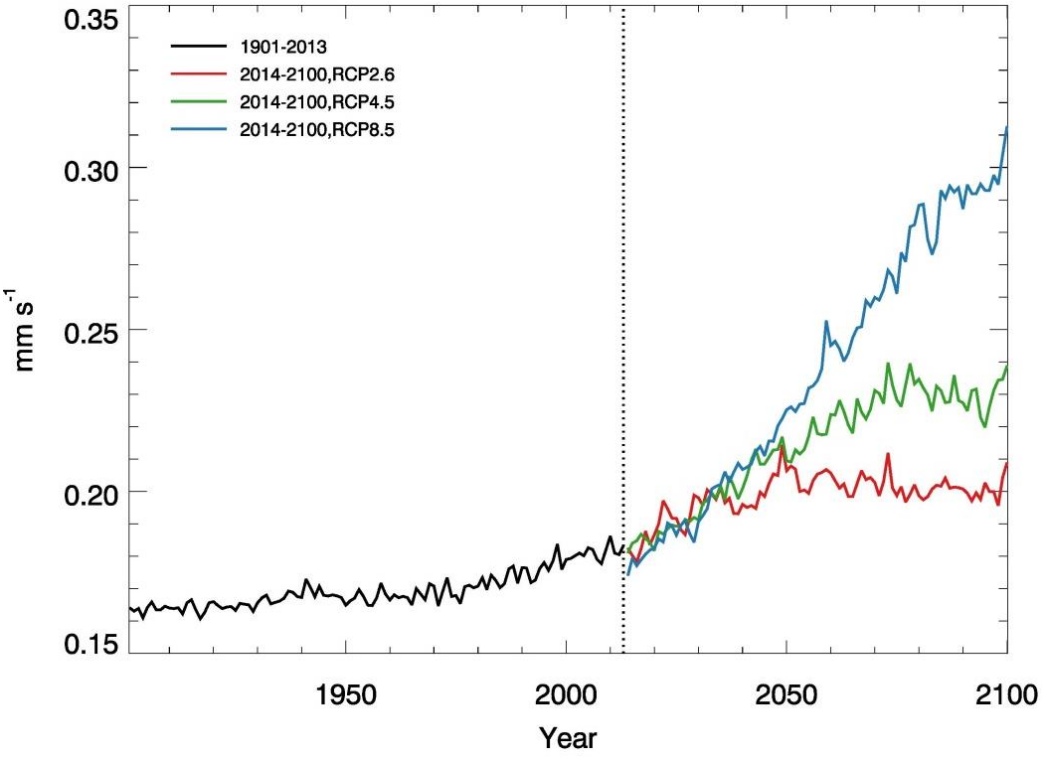

Figure 9. Global mean annual time series of CO deposition velocity (mm s^{-1}) using constant in time, spatially distributed CO concentration data during 1901-2013 (left side of dot line) and under future climate scenarios RCP2.6, RCP4.5 and RCP8.5 during 2014-2100 (right side of dot line)

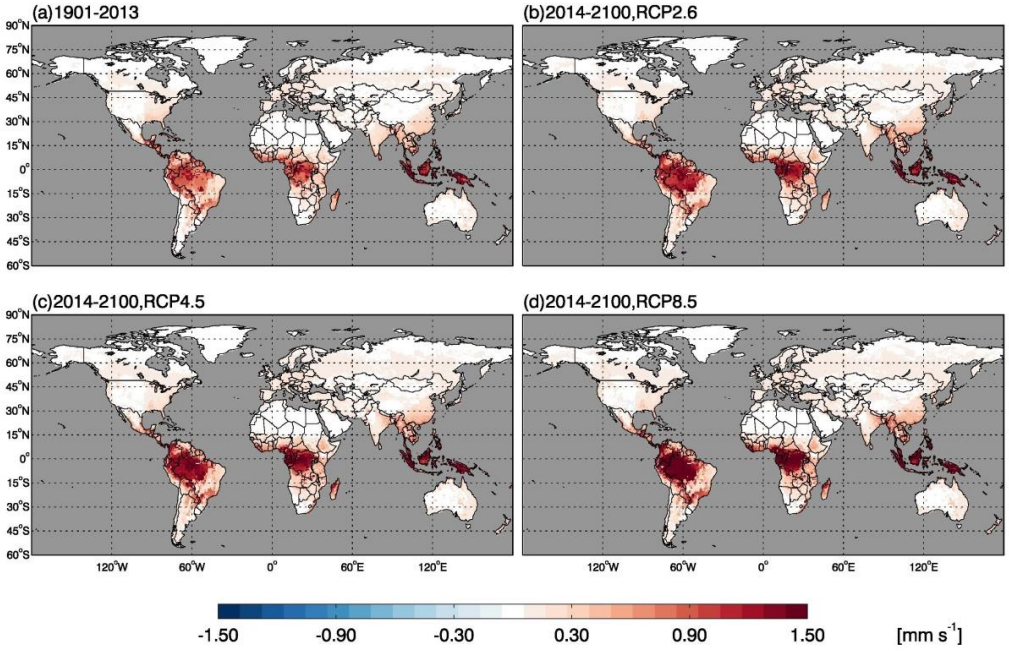

Figure 10. Global annual mean CO deposition velocity using constant in time, spatially distributed CO concentration data (mm s^{-1}) a) during 1901-2013 and b), c), d) under future climate scenarios RCP2.6, RCP4.5 and RCP8.5 during 2014-2100, respectively,

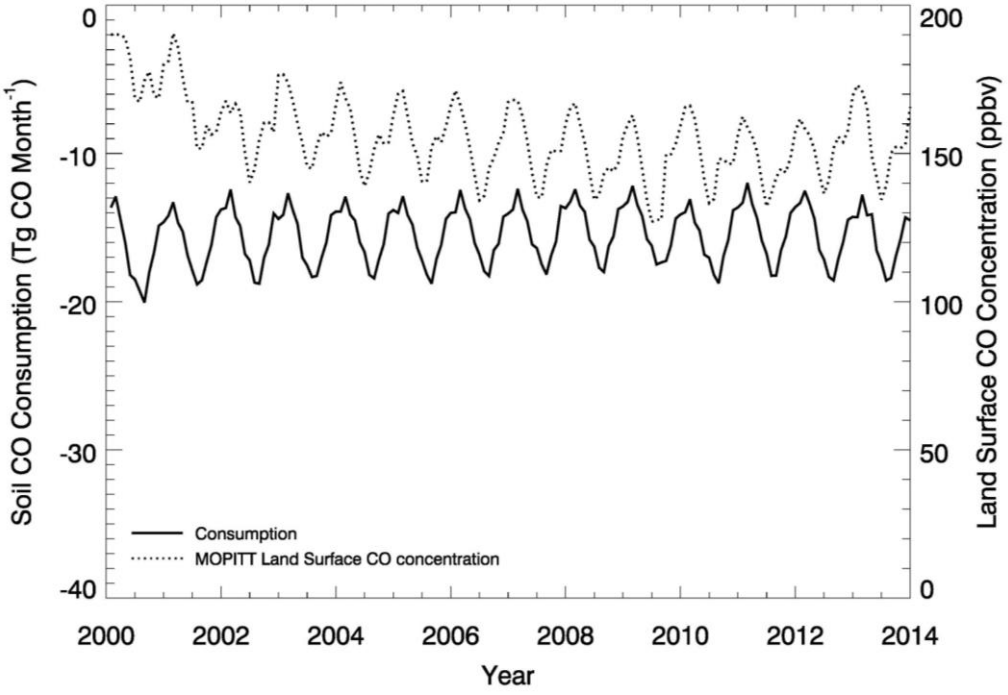

Figure 11. Global mean monthly time series of MOPITT surface atmospheric CO concentration (ppbv) and soil CO consumption from model simulations E1 (Tg CO mon^{-1})

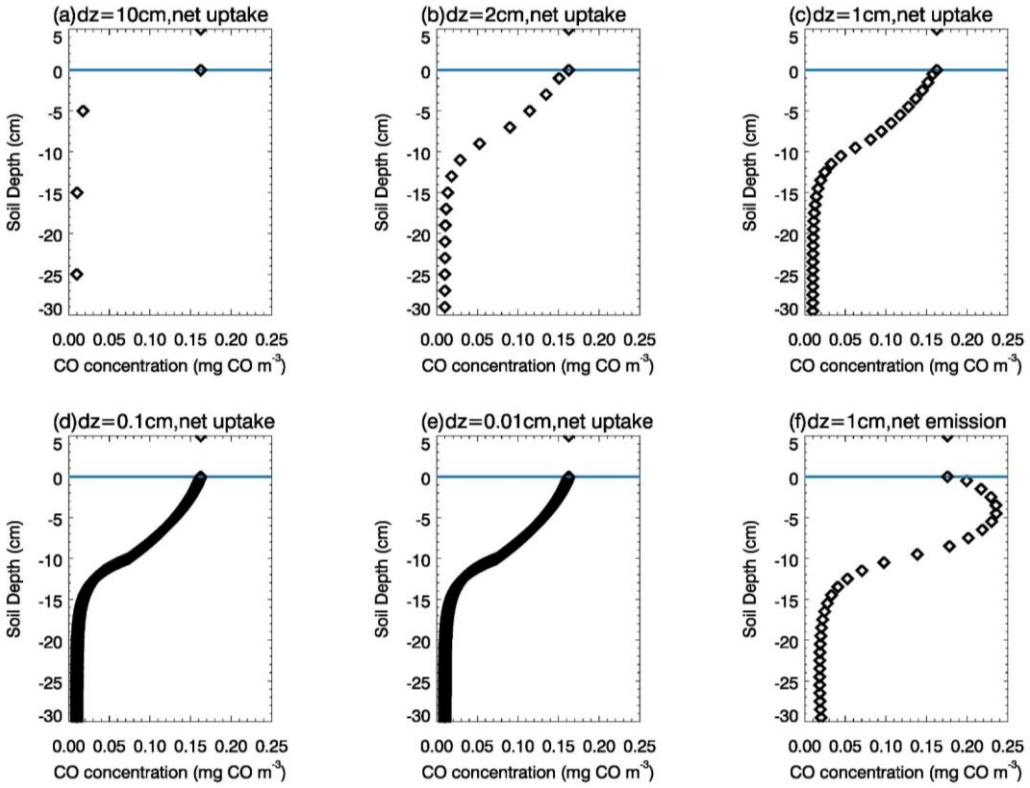

Figure 12. Daily mean vertical soil CO concentration profiles of top 30cm. In soils (depth < 0cm), black diamonds represent the soil CO concentration (mg CO m^{-3}). Above the surface (depth>=0cm), black diamonds represent atmospheric CO concentration. a), b), c), d) and e) are the results from the same day when soil is a net sink of CO but with different layer thickness (dz=10cm, 2cm, 1cm, 0.1cm and 0.01cm respectively); f) is the result from the day when soil is a net source of CO, with dz=1cm.